

# Energy Budget of Cosmological First-order Phase Transitions

José R. Espinosa<sup>a,b</sup>, Thomas Konstandin<sup>b</sup>,

José M. No<sup>c</sup> and G  raldine Servant<sup>b,c</sup>

<sup>a</sup>*ICREA, Instituci   Catalana de Recerca i Estudis Avan  ats,  
at IFAE, Universitat Aut  noma de Barcelona, 08193 Bellaterra, Barcelona, Spain*

<sup>b</sup>*CERN Physics Department, Theory Division, CH-1211 Geneva 23, Switzerland*

<sup>c</sup>*Institut de Physique Th  orique, CEA/Saclay, F-91191 Gif-sur-Yvette C  dex, France*

jose.espinosa@cern.ch, thomas.markus.konstandin@cern.ch,  
jose.miguel.no.redondo@cern.ch, geraldine.servant@cern.ch

## Abstract

The study of the hydrodynamics of bubble growth in first-order phase transitions is very relevant for electroweak baryogenesis, as the baryon asymmetry depends sensitively on the bubble wall velocity, and also for predicting the size of the gravity wave signal resulting from bubble collisions, which depends on both the bubble wall velocity and the plasma fluid velocity. We perform such study in different bubble expansion regimes, namely deflagrations, detonations, hybrids (steady states) and runaway solutions (accelerating wall), without relying on a specific particle physics model. We compute the efficiency of the transfer of vacuum energy to the bubble wall and the plasma in all regimes. We clarify the condition determining the runaway regime and stress that in most models of strong first-order phase transitions this will modify expectations for the gravity wave signal. Indeed, in this case, most of the kinetic energy is concentrated in the wall and almost no turbulent fluid motions are expected since the surrounding fluid is kept mostly at rest.

# Contents

<b>1</b>	<b>Introduction</b>	<b>1</b>
<b>2</b>	<b>Hydrodynamic relations</b>	<b>3</b>
2.1	Basic concepts . . . . .	3
2.2	Equation of state . . . . .	4
2.3	Relativistic fluid equations and bulk kinetic energy . . . . .	7
<b>3</b>	<b>Detonations, deflagrations and hybrids</b>	<b>8</b>
3.1	Detonations . . . . .	10
3.2	Deflagrations . . . . .	12
3.3	Hybrids . . . . .	13
<b>4</b>	<b>Efficiency coefficients</b>	<b>15</b>
<b>5</b>	<b>Bubble wall velocity for steady state walls</b>	<b>17</b>
5.1	EoM for the Higgs field and the friction parameter $\eta$ . . . . .	18
5.2	Wall velocity in the $(\eta, \alpha_N)$ plane . . . . .	21
5.3	Microscopic determination of $\eta$ . . . . .	23
<b>6</b>	<b>Runaway walls</b>	<b>24</b>
<b>7</b>	<b>Energy budget of first-order phase transitions</b>	<b>28</b>
<b>8</b>	<b>Summary</b>	<b>29</b>
<b>A</b>	<b>Numerical fits to the efficiency coefficients</b>	<b>32</b>

## 1 Introduction

A cosmological first-order phase transition could have far-reaching consequences and could lead to many interesting phenomena, as for example electroweak baryogenesis [1], primordial magnetic fields [2] or a stochastic background of gravitational waves [3–5]. All of them are based on the fact that a first-order phase transition proceeds by bubble nucleation and, in the process, a large portion of the available vacuum energy is stored close to the bubble walls. In all these phenomena, some essential characteristics of the first-order phase transition enter, namely the velocity of the expanding bubbles and the efficiency coefficients that keep track of the energy budget of the transition, that is, how the free energy of the Higgs field  $\phi$  initially available is distributed among bulk fluid motion, thermal energy of the plasma and gradient/kinetic energy of the Higgs field.

Quite generally, treatments of the bubble wall velocity assume that the expansion of the bubbles is hindered by some form of friction, such that the bubble wall reaches a constant speed after a rather short time of order  $\sim 1/m$ , where  $m$  represents the typical mass scale associated with the transition (i.e. electroweak mass scale in the case of the electroweak phase transition). Assuming that the free energy of the Higgs field is released into the plasma, a

hydrodynamic treatment of the plasma can be used to determine the fluid motion [6, 7]. However, as long as the microscopic mechanism of friction is unknown, this approach leaves one free parameter, typically the wall velocity. In [7] it was argued that the velocity should be fixed by the Chapman-Jouguet condition, like in chemical combustion, and this condition was subsequently used in many studies of gravitational wave production [8]. The Chapman-Jouguet condition generally leads to supersonic wall velocities with a rarefaction wave behind the bubble wall. This scenario favors gravitational wave production, since fast moving walls are essential for the production of gravitational radiation in bubble collisions [4, 5, 9–11], turbulence [12, 13] or magnetic fields [13].

Nevertheless, while being observed in chemical combustion, the Chapman-Jouguet condition is unrealistic for cosmological phase transitions [14]. To replace the Chapman-Jouguet condition, friction has been studied through a phenomenological parametrization in the Higgs equation of motion [15, 16]. Extensive simulations of hydrodynamic equations in conjunction with an equation for the Higgs field have been used to identify the stable expansion modes of the bubbles [14, 16–19]. It turns out that many solutions which are viable close to the phase transition front, where the free energy of the Higgs field is released into the plasma, are not stable globally.

The friction coefficient appearing in the Higgs equation can be determined by solving Boltzmann-type equations close to the phase transition front [15, 20]. This approach leads to subsonic wall velocities in the Standard Model (SM) and its supersymmetric extension (MSSM) and is widely used in studies of MSSM electroweak baryogenesis [21–25]. Subsonic wall velocities are crucial in electroweak baryogenesis, since this mechanism is based on diffusion of particle asymmetries into the plasma in front of the bubble wall and for a too fast wall, there is no time to build up a baryon asymmetry.

In strong first-order phase transitions, the friction exerted by the plasma on the wall might not be sufficient to prevent the bubble wall from a runaway behavior in which the wall keeps accelerating, toward ultra-relativistic velocities, as pointed out recently in [27]. We also study this runaway regime and discuss the energy balance in that case.

Our general goal in this paper is to present a unified picture of all the different regimes. We go beyond the (unjustified) Chapman-Jouguet assumption and provide general formula for the wall velocity, the fluid velocity and the efficiency factors accounting for the distribution of energy among bulk fluid motion, thermal energy of the plasma and gradient/kinetic energy of the Higgs field. The paper is organized as follows. We review the hydrodynamic treatment of the plasma in secs. 2 and 3, and subsequently obtain the efficiency coefficients in sec. 4. In sec. 5 we present a simplified treatment of the Higgs equation (a similar one has been carried out recently in [26]). We present detailed results both for the wall velocity and the efficiency coefficients that are required for the determination of gravitational wave spectra. We discuss the runaway regime in sec. 6 and summarize our results on the energy budget of first-order phase transitions in sec. 7. We conclude in sec. 8 and provide numerical fits to the efficiency coefficients in Appendix A.

## 2 Hydrodynamic relations

In this section we introduce the basic concepts and set up the notation used for the hydrodynamic analysis of the combined “wall-plasma” system [6, 7, 16].

### 2.1 Basic concepts

The energy-momentum tensor of the Higgs field  $\phi$  is given by

$$T_{\mu\nu}^\phi = \partial_\mu \phi \partial_\nu \phi - g_{\mu\nu} \left[ \frac{1}{2} \partial_\rho \phi \partial^\rho \phi - V_0(\phi) \right], \quad (1)$$

where  $V_0(\phi)$  is the renormalized vacuum potential. The energy momentum-tensor of the plasma is given by

$$T_{\mu\nu}^{plasma} = \sum_i \int \frac{d^3k}{(2\pi)^3 E_i} k_\mu k_\nu f_i(k, x), \quad (2)$$

where the sum is carried out over the species in the plasma and  $f_i(k, x)$  is the distribution function for each species. If the plasma is locally in equilibrium (perfect fluid) this can be parametrized as

$$T_{\mu\nu}^{plasma} = w u_\mu u_\nu - g_{\mu\nu} p, \quad (3)$$

where  $w$  and  $p$  are the plasma enthalpy and pressure, respectively. The quantity  $u_\mu$  is the four-velocity field of the plasma, related to the three-velocity  $\mathbf{v}$  by

$$u_\mu = \frac{(1, \mathbf{v})}{\sqrt{1 - \mathbf{v}^2}} = (\gamma, \gamma \mathbf{v}). \quad (4)$$

A constant  $\phi$  background contributes to the total pressure [see eq. (1)] and from now on we will use  $p$  for this total pressure, including such contribution.

The enthalpy  $w$ , the entropy density  $\sigma$  and the energy density  $e$  are defined by

$$w \equiv T \frac{\partial p}{\partial T}, \quad \sigma \equiv \frac{\partial p}{\partial T}, \quad e \equiv T \frac{\partial p}{\partial T} - p, \quad (5)$$

where  $T$  is the plasma temperature. One then has

$$w = e + p. \quad (6)$$

Conservation of energy-momentum is given by

$$\partial^\mu T_{\mu\nu} = \partial^\mu T_{\mu\nu}^\phi + \partial^\mu T_{\mu\nu}^{plasma} = 0. \quad (7)$$

We are primarily interested in a system with a constant wall velocity and, assuming there is no time-dependence, eq. (7) reads in the wall frame (with the wall and fluid velocities aligned in the  $z$  direction)

$$\partial_z T^{zz} = \partial_z T^{z0} = 0. \quad (8)$$

Integrating these equations across the phase transition front and denoting the phases in front and behind the wall by subscripts  $+$  (symmetric phase) and  $-$  (broken phase) one gets the matching equations (in the wall frame):

$$w_+ v_+^2 \gamma_+^2 + p_+ = w_- v_-^2 \gamma_-^2 + p_- , \quad w_+ v_+ \gamma_+^2 = w_- v_- \gamma_-^2 . \quad (9)$$

From these equations we can obtain the relations

$$v_+ v_- = \frac{p_+ - p_-}{e_+ - e_-} , \quad \frac{v_+}{v_-} = \frac{e_- + p_+}{e_+ + p_-} . \quad (10)$$

To proceed further, one needs to assume a specific equation of state (EoS) for the plasma.

## 2.2 Equation of state

Usually the plasma is well described by a relativistic gas approximation. In the symmetric phase,

$$p_+ = \frac{1}{3} a_+ T_+^4 - \epsilon , \quad e_+ = a_+ T_+^4 + \epsilon , \quad (11)$$

where  $\epsilon$  denotes the false-vacuum energy resulting from the Higgs potential (defined to be zero in the broken,  $T = 0$ , true-minimum phase). While in the broken phase

$$p_- = \frac{1}{3} a_- T_-^4 , \quad e_- = a_- T_-^4 , \quad (12)$$

with a different number of light degrees of freedom across the wall and therefore different values  $a_+$  and  $a_-$  (with  $a_+ > a_-$ ) and different temperatures on both sides of the wall. These expressions correspond to the so-called bag equation of state.

In the general case, the free energy ( $\mathcal{F} = -p$ , also called sometimes effective potential, including finite temperature corrections) of a plasma of particles with arbitrary masses  $m_i(\phi)$  is given, in the non-interacting-gas approximation, by

$$\begin{aligned} \mathcal{F} &= V_0 + \int \frac{d^3 p}{(2\pi)^3} \sum_i N_i \log [1 \mp e^{-E_i/T}] \\ &= V_0 + \frac{T^4}{2\pi^2} \sum_i N_i Y_{b/f}(m_i/T) , \end{aligned} \quad (13)$$

where  $V_0$  is the  $T = 0$  effective potential,  $E_i^2 = p^2 + m_i^2$ ,

$$Y_{b/f}(x) = \int_0^\infty dy y^2 \log[1 \mp \exp(-\sqrt{x^2 + y^2})], \quad (14)$$

the  $-/+$  signs in the last equation hold for bosons/fermions, the index  $i$  denotes the different species and  $N_i$  the internal degrees of freedom (that in this notation is negative for fermions). Species that are light compared to  $T$  behave as a relativistic gas while species much heavier than  $T$  are Boltzmann suppressed in the plasma and can be neglected. As is well known,

for small  $m_i/T$  the function  $Y_{b/f}$  tends to a constant ( $-\pi^4/45$  for bosons and  $7\pi^4/360$  for fermions) so that  $a_{\pm}$  in the bag EoS are explicitly given by

$$a_{\pm} = \frac{\pi^2}{30} \sum_{\text{light } i} \left[ N_i^b + \frac{7}{8} |N_i^f| \right] ; \quad (15)$$

while for large  $m_i/T$  one has  $Y_{b/f}(m_i/T) \sim \pm \exp(-m_i/T)$ . Hence, only particles that have masses comparable to  $T$  can cause deviations from the bag EoS. In many cases this deviation is small because the free-energy is dominated by a large number of light degrees of freedom. For example in the Standard Model, the  $W^{\pm}$  and  $Z^0$  bosons contribute to this deviation from the bag EoS (and to a lesser extent the tops) but altogether the modification in the energy density is at the percent level and hence small.

If the deviations from the bag EoS are not so small one can still parametrize the plasma behavior in terms of quantities that mimic the bag EoS ones. In particular, from the free-energy ( $\mathcal{F} = -p$ ) we can define

$$a_{\pm} \equiv \frac{3}{4T_{\pm}^3} \left. \frac{\partial p}{\partial T} \right|_{\pm} = \frac{3\omega_{\pm}}{4T_{\pm}^4} , \quad \epsilon_{\pm} \equiv \frac{1}{4}(e_{\pm} - 3p_{\pm}) . \quad (16)$$

In the special case of bag EoS, these definitions reproduce the correct  $a_{\pm}$  and give  $\epsilon_+ = \epsilon$  and  $\epsilon_- = 0$ . In terms of these quantities one can write

$$p_{\pm} = \frac{1}{3}a_{\pm}T_{\pm}^4 - \epsilon_{\pm} , \quad e_{\pm} = a_{\pm}T_{\pm}^4 + \epsilon_{\pm} , \quad (17)$$

but now  $a_{\pm}$  and  $\epsilon_{\pm}$  are  $T$ -dependent quantities and should be interpreted with some care. By their definition (16) they satisfy:

$$\frac{\partial \epsilon_{\pm}}{\partial T_{\pm}} = \frac{T_{\pm}^4}{3} \frac{\partial a_{\pm}}{\partial T_{\pm}} . \quad (18)$$

There is a certain arbitrariness in the definition of  $a_{\pm}$  but ours is especially convenient because some formulas we discuss in sect. 5 can be easily generalized even if the bag EoS is not valid.

Using the bag equations of state (11) and (12) in eq. (10) we get

$$\begin{aligned} v_+ v_- &= \frac{1 - (1 - 3\alpha_+)r}{3 - 3(1 + \alpha_+)r} , \\ \frac{v_+}{v_-} &= \frac{3 + (1 - 3\alpha_+)r}{1 + 3(1 + \alpha_+)r} , \end{aligned} \quad (19)$$

where we defined

$$\alpha_+ \equiv \frac{\epsilon}{a_+ T_+^4} , \quad r \equiv \frac{a_+ T_+^4}{a_- T_-^4} . \quad (20)$$

The quantity  $\alpha_+$  is the ratio of the vacuum energy to the radiation energy density and typically characterizes the “strength” of the phase transition: the larger  $\alpha_+$  the stronger the phase transition. These two equations can be combined to give

$$v_+ = \frac{1}{1 + \alpha_+} \left[ \left( \frac{v_-}{2} + \frac{1}{6v_-} \right) \pm \sqrt{\left( \frac{v_-}{2} + \frac{1}{6v_-} \right)^2 + \alpha_+^2 + \frac{2}{3}\alpha_+ - \frac{1}{3}} \right] , \quad (21)$$

so that there are two branches of solutions, corresponding to the  $\pm$  signs in eq. (21). In the general case, with some deviation from the bag EoS, eqs. (19) and (21) still apply, with  $r$  defined as before and  $\alpha_+ \equiv (\epsilon_+ - \epsilon_-)/(a_+ T_+^4)$ .

Figure 1 shows these solutions for several values of  $\alpha_+$ . The first branch (with positive sign) gives solutions of detonation type,  $v_+ > v_-$ , corresponding to  $r < \frac{1}{1+3\alpha_+}$ . The function  $v_+$  has a minimum at  $v_- = c_s$ . Notice that the point  $v_+ = v_- = 1$  is always a solution of this kind, with  $r = \frac{1}{1+3\alpha_+}$ ; besides, in the limit  $r \rightarrow 0$  one obtains  $v_+ = 1$  and  $v_- = 1/3$ . The second branch of solutions exists only if  $\alpha_+ < 1/3$ , and is of deflagration type,  $v_+ < v_-$  (it ranges over all values of  $v_-$ ). Also for deflagrations, the function  $v_+$  has an extremum at  $v_- = c_s$ ; the endpoint,  $v_- = 1$ , is given by the limit  $r \rightarrow \infty$  and yields  $v_+ = \frac{1-3\alpha_+}{3+3\alpha_+}$ . The limiting case  $\alpha_+ = 0$  corresponds to  $v_+ v_- = 1/3$ , connects both regions and will be relevant for the discussion of shock fronts in the next section.

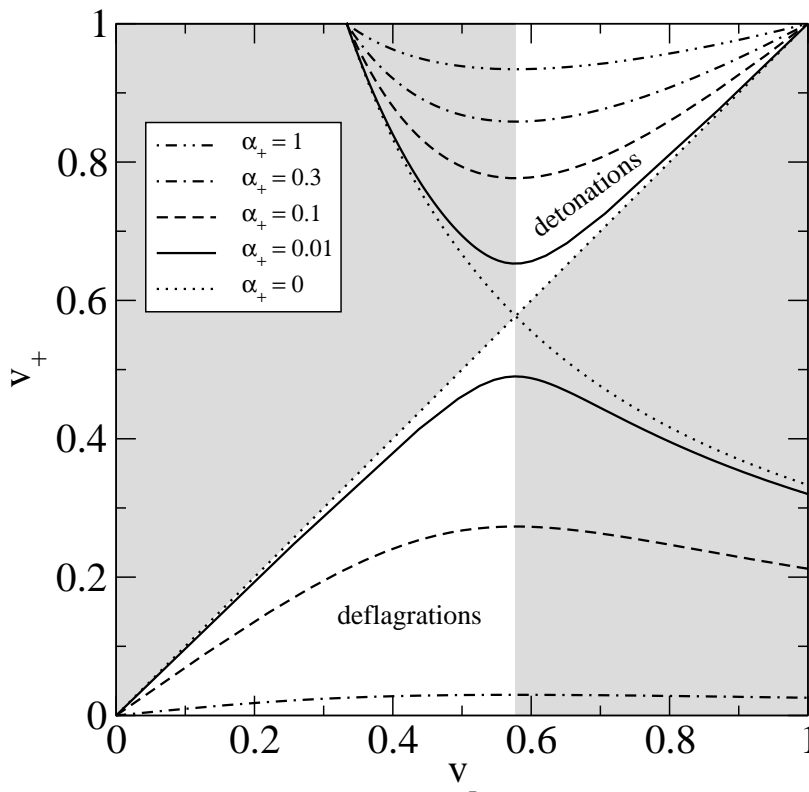


Figure 1: Contours of the fluid velocities  $v_+$  and  $v_-$  in the wall frame for fixed  $\alpha_+$ . In the shaded region in the top-left no consistent solutions to hydrodynamic equations exist. Flow profiles in the shaded region in the bottom-right decay into hybrid solutions, with  $v_- = c_s^-$  (see sect. 3.3).

To determine all relevant quantities in terms of the phase transition parameters, one still has to determine one of the two velocities, or equivalently, relate  $T_+$  to  $T_-$ ; this will be the subject of sec. 5. Before doing so, we want to provide a more detailed description and a physical understanding of the above solutions as well as of the hybrid regime. Hence, for now, we treat the wall velocity as a free parameter, without any further assumptions about the microscopic properties of the plasma. In sections 3 and 4 we present the analysis of

the different types of solutions for the motion of the plasma fluid. We will be particularly interested in the efficiency factor  $\kappa$  (that measures how much of the vacuum energy goes into bulk kinetic energy and is a crucial quantity to determine gravitational wave production) as a function of the wall velocity. To define  $\kappa$ , we first need the relativistic fluid equations for the plasma that we derive now.

## 2.3 Relativistic fluid equations and bulk kinetic energy

The starting point are the continuity equations (7) that, for a general plasma of form (3), read (see e.g. [6])

$$\partial_\mu T^{\mu\nu} = u^\nu \partial_\mu (u^\mu w) + u^\mu w \partial_\mu u^\nu - \partial^\nu p. \quad (22)$$

Projecting along the flow then leads, using  $u_\mu \partial_\nu u^\mu = 0$ , to

$$\partial_\mu (u^\mu w) - u_\mu \partial^\mu p = 0. \quad (23)$$

Consider next the projection perpendicular to the flow with some space-like vector  $\bar{u} = \gamma(v, \mathbf{v}/v)$  such that  $\bar{u}_\mu u^\mu = 0$ ,  $\bar{u}^2 = -1$ . This turns (22) into the relativistic Euler equation

$$\bar{u}^\nu u^\mu w \partial_\mu u_\nu - \bar{u}^\nu \partial_\nu p = 0. \quad (24)$$

In the following we assume a spherically symmetric configuration. Additionally, because there is no characteristic distance scale in the problem, the solution should be a similarity solution that depends only on the combination  $\xi = r/t$  where  $r$  is the distance from the center of the bubble and  $t$  is the time since nucleation.<sup>1</sup>  $\xi$  is thus the velocity of a given point in the wave profile and the particles at the point described by  $\xi$  in the wave profile move with velocity  $v(\xi)$ , which is therefore the fluid velocity in the frame of the bubble center. This turns the different gradients into

$$u_\mu \partial^\mu = -\frac{\gamma}{t}(\xi - v) \partial_\xi, \quad \bar{u}_\mu \partial^\mu = \frac{\gamma}{t}(1 - \xi v) \partial_\xi. \quad (25)$$

Finally, this yields for eqs. (23) and (24)

$$\begin{aligned} (\xi - v) \frac{\partial_\xi e}{w} &= 2 \frac{v}{\xi} + [1 - \gamma^2 v(\xi - v)] \partial_\xi v, \\ (1 - v\xi) \frac{\partial_\xi p}{w} &= \gamma^2 (\xi - v) \partial_\xi v. \end{aligned} \quad (26)$$

The derivatives  $\partial_\xi e$  and  $\partial_\xi p$  can be related through the speed of sound in the plasma,  $c_s^2 \equiv (dp/dT)/(de/dT)$ , so as to get the central equation describing the velocity profile:

$$2 \frac{v}{\xi} = \gamma^2 (1 - v\xi) \left[ \frac{\mu^2}{c_s^2} - 1 \right] \partial_\xi v, \quad (27)$$

with  $\mu$  the Lorentz-transformed fluid velocity

$$\mu(\xi, v) = \frac{\xi - v}{1 - \xi v}. \quad (28)$$

---

<sup>1</sup> The matching equations (9) can also be derived using energy-momentum conservation for similarity solutions in the rest frame.



In general,  $c_s^2$  depends on the EoS for the plasma, being  $c_s^2 = 1/3$  in the bag case. In the general case,  $c_s^2$  will be  $\xi$ -dependent, although in many cases of interest deviations from  $1/3$  will be small.

Eq. (27) can then be solved (with the appropriate boundary conditions) to yield the velocity profile  $v(\xi)$  of the plasma. Subsequently, eqs. (26) can be integrated to yield

$$w(\xi) = w_0 \exp \left[ \int_{v_0}^{v(\xi)} \left( 1 + \frac{1}{c_s^2} \right) \gamma^2 \mu dv \right]. \quad (29)$$

In the calculation of the gravitational radiation produced in the phase transition one needs to compute the kinetic energy in the bulk motion of the plasma. We have now all ingredients necessary to perform such calculation. The ratio of that bulk kinetic energy over the vacuum energy gives the efficiency factor  $\kappa$  as

$$\kappa = \frac{3}{\epsilon \xi_w^3} \int w(\xi) v^2 \gamma^2 \xi^2 d\xi, \quad (30)$$

where  $\xi_w$  is the velocity of the bubble wall. Notice that this definition coincides with the expression used in the gravitational wave literature, that is given by  $\kappa = \frac{3}{\epsilon R_w^3} \int w v^2 \gamma^2 R^2 dR$ , but differs from the definition used in ref. [5] by a factor  $\xi_w^3$ .

We also numerically check energy conservation: Integration of  $T_{00}$  over a region larger than the bubble (including the shock front) is constant in time, giving

$$\int \left[ \left( \gamma^2 - \frac{1}{4} \right) w - \frac{3}{4} w_N \right] \xi^2 d\xi = \frac{\epsilon}{3} \xi_w^3, \quad (31)$$

where  $w_N$  denotes the enthalpy at nucleation temperature far in front of the wall. This implies that the energy which is not transformed into kinetic bulk motion, but is used instead to increase the thermal energy, is

$$1 - \kappa = \frac{3}{\epsilon \xi_w^3} \int \frac{3}{4} (w - w_N) \xi^2 d\xi = \frac{3}{\epsilon \xi_w^3} \int (e - e_N) \xi^2 d\xi. \quad (32)$$

### 3 Detonations, deflagrations and hybrids

We can now use the previous fluid equations to describe the different kinds of solutions for the motion of the plasma disturbed by the moving phase transition wall. In the discussion below, the sound velocity in the plasma plays a very relevant role. This velocity will in general depend on  $\xi$  and it is convenient to distinguish its asymptotic values in the symmetric and broken phases. We denote those two velocities by  $c_s^\pm$ . In many cases, we expect the bag EoS to hold in the symmetric phase and therefore  $c_s^+ = 1/\sqrt{3}$ .

Before embarking in the discussion of the different types of velocity profiles, it proves useful to study first in more detail the profile eq. (27) without worrying about physical boundary conditions. The different curves in Fig. 2 are obtained by solving for  $\xi$  as a function of  $v$  [instead of the more physically meaningful  $v(\xi)$ , the plasma velocity profile] using arbitrary boundary conditions and setting  $c_s = 1/\sqrt{3}$ . This procedure has the advantage that  $\xi(v)$  is

a single-valued function. The meaning of the different regions will be explained later on. We see two different fixed points: one for  $\xi = c_s$  and  $v = 0$  and the other for  $\xi = v = 1$ . This structure of fixed points can be understood analytically in a simple way by introducing an auxiliary quantity  $\tau$  to describe parametrically these curves in the plane  $(\xi, v)$ . Using such parameter, eq. (27) can be split in the two simpler equations

$$\begin{aligned}\frac{dv}{d\tau} &= 2vc_s^2(1-v^2)(1-\xi v) , \\ \frac{d\xi}{d\tau} &= \xi[(\xi-v)^2 - c_s^2(1-\xi v)^2] ,\end{aligned}\tag{33}$$

which clearly display the mentioned fixed points. The point  $(c_s, 0)$  is in fact what is technically called an improper node and all curves approach it tangentially to the  $v = 0$  line. One also sees that  $dv/d\tau > 0$  so that along each curve  $v$  grows monotonically with  $\tau$ . In the more general case with a  $\xi$ -dependent  $c_s$  deviating somewhat from  $1/\sqrt{3}$  one expects quantitative changes in these curves but the same qualitative behavior [with the fixed point at  $(c_s^-, 0)$ ].

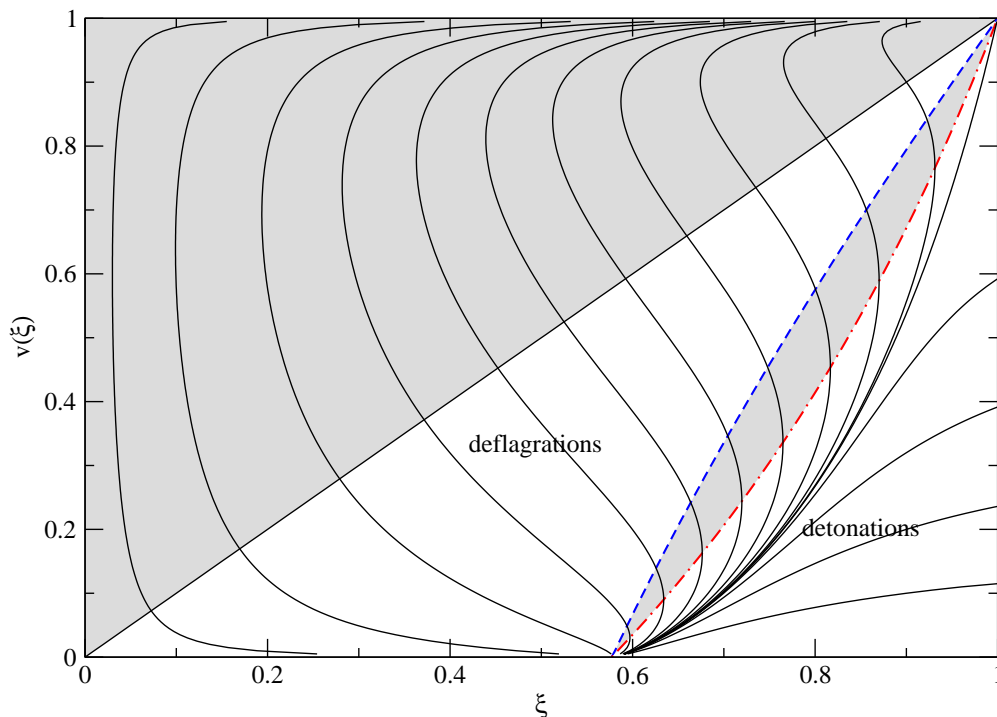


Figure 2: General profiles of the fluid velocity  $v(\xi)$  in the frame of the bubble center (with  $c_s^2 = 1/3$ ). Detonation curves start below  $\mu(\xi, v) = c_s$  (dashed-dotted curve) and end at  $(\xi, v) = (c_s, 0)$ . Deflagration curves start below  $v = \xi$  and end at  $\mu(\xi, v)\xi = c_s^2$  (dashed curve) corresponding to the shock front, as explained in the text. There are no consistent solutions in the shaded regions.

Physical velocity profiles for expanding bubbles have to go to zero at some distance in front and behind the bubble wall and, in view of Fig. 2, this clearly requires some discontinuous jump, which usually can take place right at the phase transition front, where many other quantities also jump. The different types of possible velocity profiles that result are discussed next.

### 3.1 Detonations

A pictorial representation of a typical detonation is depicted in Fig. 3, right plot. The corresponding velocity profile is as in Fig. 4, lower left plot. More precisely, in detonations the phase transition wall moves at supersonic speed  $\xi_w$  ( $\xi_w > c_s^+$ ) hitting fluid that is at rest in front of the wall. In the wall frame, the symmetric-phase fluid is moving into the wall at  $v_+ = \xi_w$  and entering the broken phase behind the wall where it slows down so that  $v_- < v_+$ . In the rest frame of the bubble center, the fluid velocity right after the wall passes jumps to  $v(\xi_w) = \mu(v_+, v_-)$  (the Lorentz transformation (28) from the frame of the wall to the rest frame of the center of the bubble) and then slows down until it comes to a stop, at some  $\xi < \xi_w$ , forming a rarefaction wave behind the wall. From the previous discussion we know that  $v$  will go to zero smoothly at  $\xi = c_s^-$ .

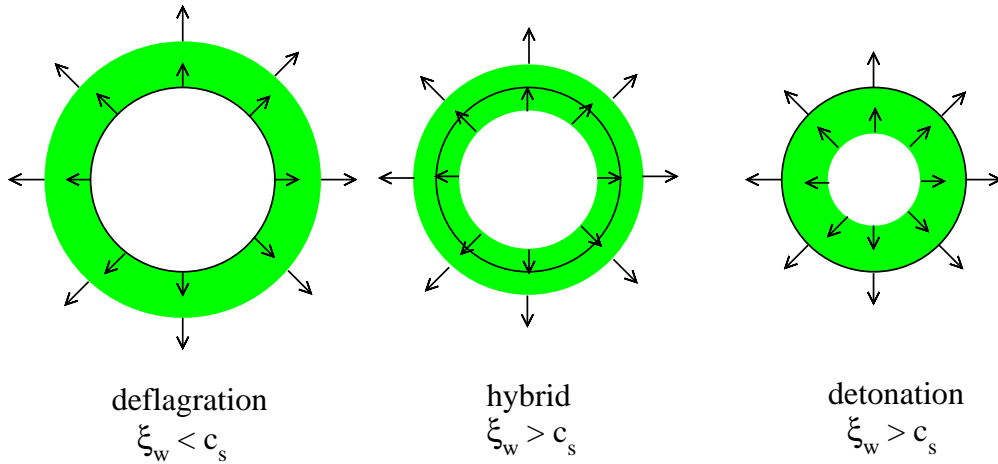


Figure 3: Pictorial representation of expanding bubbles of different types. The black circle is the phase interface (bubble wall). In green we show the region of non-zero fluid velocity.

In order to obtain a consistent solution in the region  $c_s^- < \xi < \xi_w$ , one needs  $0 < \partial_\xi v < \infty$  which, using eq. (27), requires  $\mu(\xi) > \mu(\xi_w) \geq c_s^-$  behind the wall. Consequently, detonation solutions are confined to the lower right corner of fig. 2, as indicated. Boosting to the wall frame this implies  $v_- \geq c_s^-$ , since  $v_- = \mu(\xi_w, v(\xi_w))$ . Therefore, detonations can be divided into Jouguet detonations ( $v_- = c_s^-$ ) and weak detonations ( $v_- > c_s^-$ ); strong detonations ( $v_- < c_s^-$ ) are not consistent solutions of the fluid equations, see fig. 1.<sup>2</sup>

Fig. 4 shows also the enthalpy profile (bottom right) for a detonation. Concerning this profile, remember that the matching conditions across the wall give

$$w_N = w_+ = w_- \left( \frac{1 - \xi_w^2}{\xi_w} \right) \left( \frac{v_-}{1 - v_-^2} \right), \quad (34)$$

where the subscript  $N$  denotes the plasma at the temperature of nucleation far in front of

---

<sup>2</sup>As  $c_s^-$  can be different from  $1/\sqrt{3}$  in the most general case, the forbidden region  $v_- < c_s^-$ , shaded in Fig. 1, will be shifted in those cases.

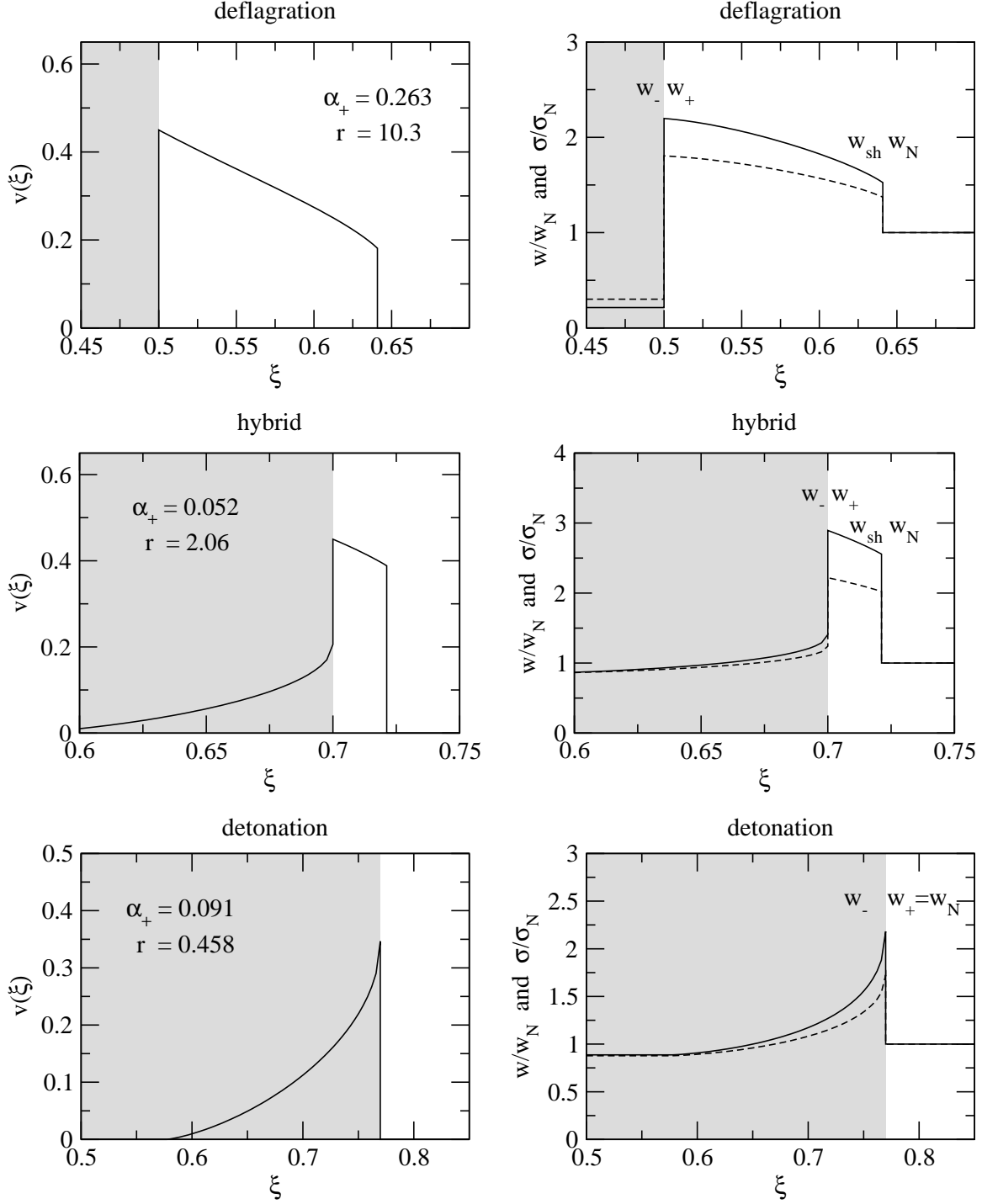


Figure 4: Examples of the fluid velocity (in the plasma rest frame), enthalpy and entropy profiles for a subsonic deflagration, a deflagration with rarefaction wave (hybrid) and a detonation, for  $a_-/a_+ = 0.85$ . The bubble of broken phase is in gray. For detonations, the fluid kinetic energy and thermal energy are concentrated near the wall but behind it i.e. inside the bubble, while they are located outside (mostly outside) of the bubble for deflagrations (hybrids).

the wall. Then, eq. (29) transforms into

$$w(\xi) = w_N \left( \frac{\xi_w}{1 - \xi_w^2} \right) \left( \frac{1 - v_-^2}{v_-} \right) \exp \left[ - \int_{v(\xi)}^{v(\xi_w)} \left( 1 + \frac{1}{c_s^2} \right) \gamma^2 \mu dv \right]. \quad (35)$$

Similar formulas can be derived for other quantities like the entropy (also shown in fig. 4), the temperature, etc. It is straightforward to show that

$$T_- > T_+ = T_N . \quad (36)$$

by using the detonation condition  $r < 1/(1 + 3\alpha_+)$ .

### 3.2 Deflagrations

A pictorial representation of a typical deflagration is depicted in Fig. 3, left plot. The corresponding velocity profile is as in Fig. 4, upper left plot. In contrast with detonations, in deflagrations the plasma is at rest right behind the wall, so that the wall velocity is now  $\xi_w = v_-$ . These solutions correspond to the lower branches in Fig. 1, with a fluid velocity that is larger behind the wall than in front,  $v_- > v_+$ . From Fig. 1 we also see that in this case the hydrodynamic relations across the wall imply  $v_+ < c_s$ . The fluid velocity just in front of the wall jumps to  $v(\xi_w) = \mu(v_-, v_+)$ . As  $v_- > v_+$ , we get  $v(\xi_w) < \xi_w$ , so that the profile of deflagration solutions start below the line  $v = \xi$ , as indicated in fig. 2.

As one moves out in  $\xi$ ,  $v(\xi)$  decreases and eventually would become double-valued before reaching zero<sup>3</sup>. Now we cannot accommodate the required jump to zero velocity using the phase transition front, which is already fixed at the beginning of the velocity profile. The way out of this dilemma is that the flow can drop to zero in a shock-front: we can use eq. (19) where now quantities with subscript  $\pm$  denote the two sides of the shock-front instead of the phase transition wall. (Notice also that the shock occurs in the symmetric phase where in general we can assume the bag EoS holds.) At the shock-front there is no discontinuity in  $\epsilon$ , and therefore  $\alpha_+ = 0$ , yet a discontinuity in velocities is possible. As given by eq. (19) and shown in Fig. 1, this requires [17] that the inward and outward velocities of the fluid in the shock-front rest-frame fulfill the relation  $v_+ v_- = 1/3$ , which in the plasma rest frame translates to  $\mu(\xi_{sh}, v_{sh}) \xi_{sh} = c_s^2$ . This condition determines the position of the shock front, which can be seen to occur before the singular point  $\mu(\xi, v(\xi)) = c_s$  (where  $dv/d\xi \rightarrow -\infty$ ) is reached, see fig. 2.

Fig. 4 also shows the enthalpy and entropy profiles (top right) for a deflagration. Notice that the temperature  $T_+$  in this case does not coincide with the temperature of the plasma outside the shock  $T_N$ , since thermodynamic quantities are changing in front of the wall and also at the shock front discontinuity. [For the same reason, explicit formulas like (35) would be now more involved.] As illustrated by the plots in Fig. 4 one always has the inequality  $\omega_+ > \omega_N$ , i.e.  $a_+ T_+^4 > a_N T_N^4$ . In fact, for deflagrations one always has the inequalities

$$T_+ > T_{sh} > T_N > T_- \quad (37)$$

although the last one depends on the details of the Higgs equation of motion, discussed in sect. 5. Hence the limit  $\alpha_+ < 1/3$ , that one found for  $\alpha_+ = \epsilon/(a_+ T_+^4)$  in deflagrations, translates into a weaker bound on the ratio  $\alpha_N = \epsilon/(a_N T_N^4)$  as  $\alpha_N > \alpha_+$ .

An upper limit on  $\alpha_N$  will be important later on to set an upper limit on  $\eta$ . How large can  $\alpha_N$  be for a fixed wall velocity? From  $\alpha_+ < 1/3$  we get the upper bound  $\alpha_N < \omega_+/(3\omega_N)$

---

<sup>3</sup>In spite of appearances, this happens even for very low values of the starting  $v(\xi)$  due to the improper-node nature of the point  $(c_s, 0)$  (see discussion above).

and the ratio  $\omega_+/\omega_N$  cannot be made arbitrarily large. Inspection of the deflagration profiles in Fig. 2 shows that  $\omega_+/\omega_N$  will be maximized by the case with strongest shock-front, which corresponds to the highest possible  $v(\xi_w)$ , that is,  $v(\xi_w) = \xi_w$ . In the wall frame this gives  $v_+ = 0$  and, using the matching conditions (9), this case also has  $\omega_- \rightarrow 0$ , *i.e.*  $a_- T_-^4 \rightarrow 0$ . Physically this would represent a limiting case for which the transition is such that the broken phase inside the bubble is empty: the plasma is swept away by the wall (thus leading to the strongest possible shock-front) and larger values of  $\eta$  cannot be realized microscopically. The same matching conditions also give us  $\omega_+ \rightarrow 4\epsilon$ , which represents a fixed upper bound for  $\omega_+$ . Going now to the shock rest frame and matching there one gets  $\omega_N = \omega_{sh} c_s^2 (1 - \xi_{sh}^2) / (\xi_{sh}^2 - c_s^4)$ . The quantities  $\omega_{sh}$  and  $\xi_{sh}$  can be obtained once the boundary condition  $v(\xi_w) = \xi_w$  is fixed and lead to the minimal value of  $\omega_N$ . The resulting upper bound on  $\alpha_N$  can be fitted numerically as a function of the wall velocity, and one gets

$$\alpha_N^{max}|_{\text{defla.}} \simeq \frac{1}{3} \frac{1}{(1 - \xi_w)^{-13/10}}, \quad (38)$$

as derived in Appendix A.

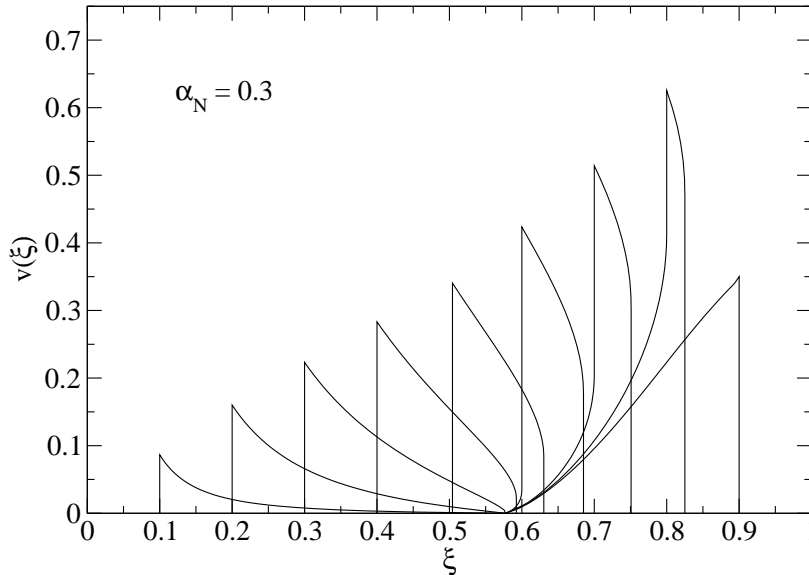


Figure 5: Fluid velocity profiles (in the plasma rest frame) for deflagrations, hybrids and detonations, for different wall velocities and  $\alpha_N = 0.3$ .

### 3.3 Hybrids

From the previous discussion of velocity jumps it is clear that it should be possible to combine detonation and deflagration solutions into a new velocity profile that is a superposition of both types (thus the name hybrid), provided the wall is supersonic. In fact, it is known from hydrodynamics simulations [19] that supersonic deflagrations are not stable but develop a rarefaction wave, identical to the detonation profile discussed earlier. A pictorial representation of a typical hybrid bubble is depicted in Fig. 3, central plot. The corresponding

velocity profile is shown in Fig. 4, middle left plot. Applying the hydrodynamic constraints for deflagration and detonation solutions we have (see fig. 1)  $\mu(\xi_w, v(\xi_w^-)) = v_- \geq c_s^-$  and  $\mu(\xi_w, v(\xi_w^+)) = v_+ \leq c_s^+$ . On the other hand, entropy considerations enforce  $v_- \leq c_s^-$ , so that the rarefaction wave has to be of Jouguet type, with  $v_- = c_s^-$ .

Therefore in these hybrid solutions the wall velocity  $\xi_w$  is not identified with either  $v_+$  or  $v_-$ , and the phase transition front is followed by a rarefaction wave of Jouguet type ( $\xi_w > v_- = c_s^- > v_+$ ) and is preceded by a shock front. Typical enthalpy and entropy profiles are shown in the middle right plot of Fig. 4. As the wall velocity increases, the deflagration part of the solution becomes thinner, and eventually disappears, as shown in Fig. 5.

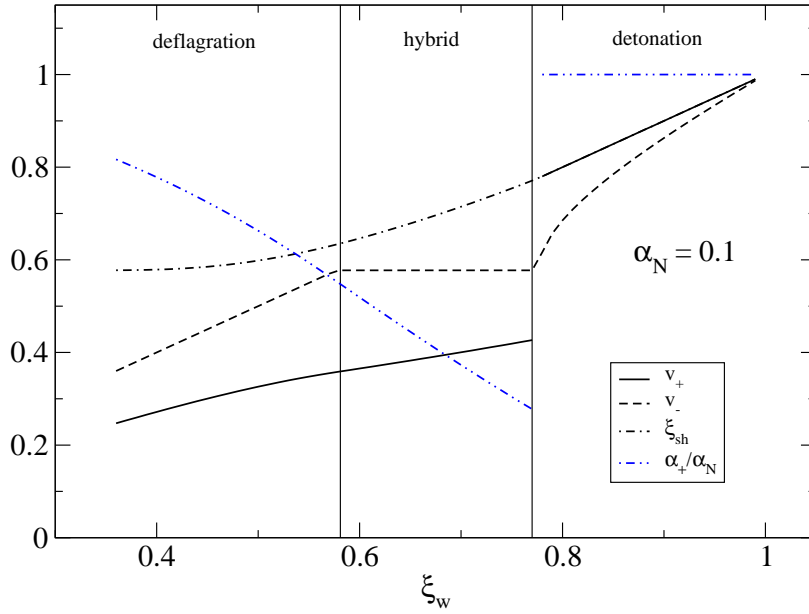


Figure 6: The flow velocities in the wall frame,  $v_+$  and  $v_-$ , the velocity of the shock front  $\xi_{sh}$  and the ratio  $\alpha_+/\alpha_N$  as a function of the wall velocity (for  $\alpha_N = 0.1$ ).

In summary, one obtains the following picture. For subsonic wall velocities, the bubble expansion proceeds in general by deflagrations. If for constant  $\alpha_N$  the wall velocity is increased beyond the velocity of sound, the flow profile develops a rarefaction wave. If the wall velocity is further increased, the shock becomes thinner until it completely vanishes and the bubble expansion proceeds by a Jouguet detonation. When the shock front vanishes, some of the quantities right in front of the wall experience a jump, namely the temperature  $T_+$ , the flow velocity  $v_+$  and also  $\alpha_+$  as illustrated in Fig. 6. Beyond this point the solutions are given by weak detonations ( $v_- > c_s^-$ ). The hybrid solutions then fill the gap of wall velocities between Jouguet deflagrations and Jouguet detonations [19], as seen in Fig. 7 which gives the maximal flow velocity in the plasma rest frame as a function of the wall velocity  $\xi_w$  for fixed values of  $\alpha_N$ . For deflagrations and hybrids the maximal flow is in front of the wall while for detonations it is behind it. Notice that, in the transition from hybrids to detonations, the maximal flow velocity jumps without a gap in  $\xi_w$ . The whole flow profile can be

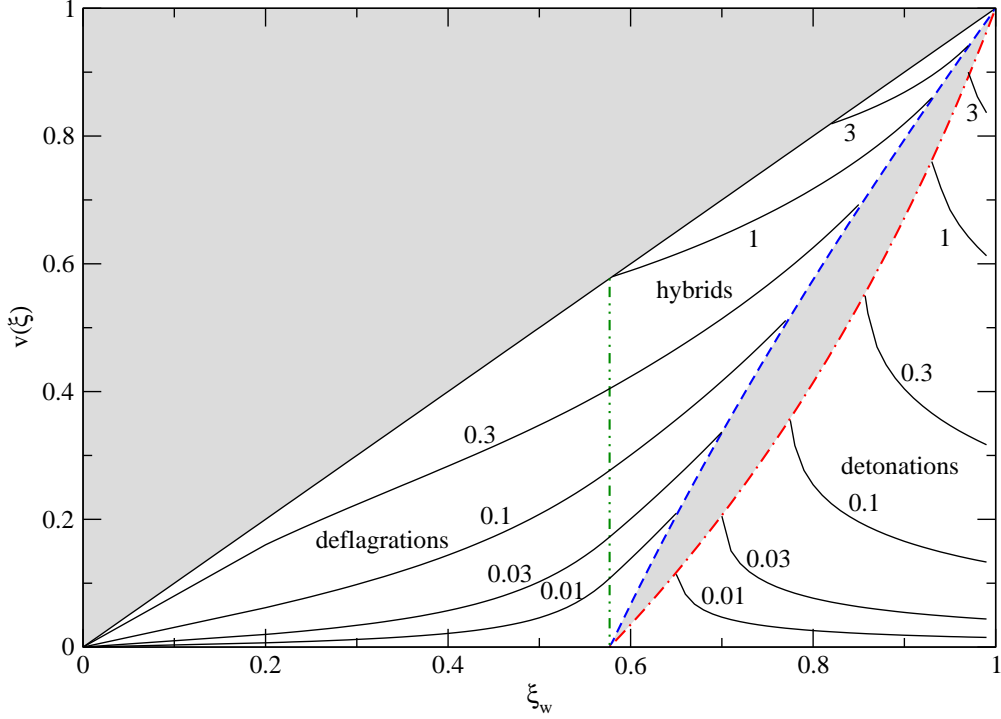


Figure 7: The maximal flow velocity in the plasma rest frame as a function of the wall velocity and several values of  $\alpha_N$ , as indicated by the labels of each curve.

reconstructed using Fig. 2.

## 4 Efficiency coefficients

In the following we present the analysis of the efficiency coefficient  $\kappa$  (the ratio of bulk kinetic energy to vacuum energy) following ref. [6, 17, 5]. Steinhardt argued in his seminal work [7] that the relative plasma velocity behind the wall should just be given by the speed of sound,  $v_- = c_s^-$ . Using this piece of information in eq. (19) gives immediately

$$\xi_w = \xi_J \equiv \frac{\sqrt{\alpha_+(2 + 3\alpha_+)} + 1}{\sqrt{3}(1 + \alpha_+)} \quad (\text{Jouguet detonations}), \quad (39)$$

and

$$\kappa \simeq \frac{\sqrt{\alpha_N}}{0.135 + \sqrt{0.98 + \alpha_N}} \quad (\text{Jouguet detonations}). \quad (40)$$

Notice that this differs from the result in ref. [5] due to our different definition of the efficiency factor  $\kappa$  [see discussion after eq. (30)].

As already mentioned, the Jouguet condition turns out to be unrealistic in cosmological phase transitions [19], and therefore one needs to rederive a formula for  $\kappa$  that supersedes eq. (40). In the next section we will discuss how to relate the two velocities in the plasma  $v_+$  and  $v_-$  (which is equivalent to the determination of the bubble wall). Knowing the wall



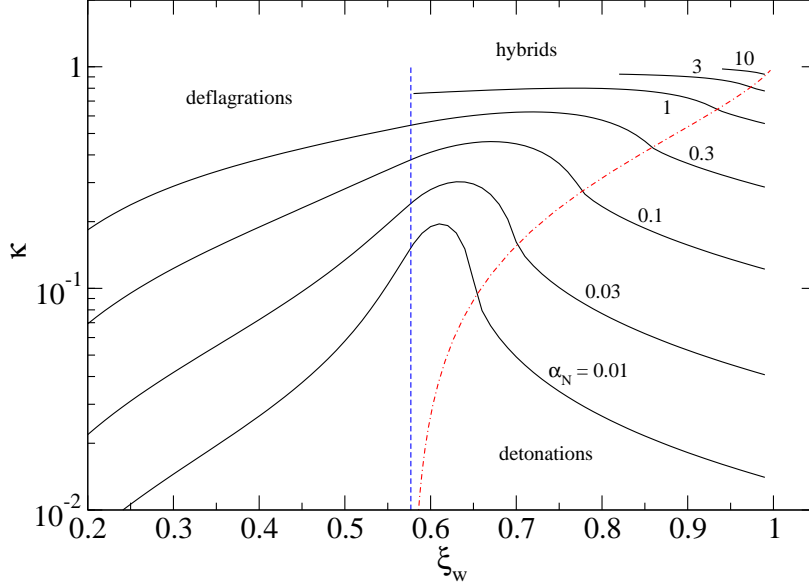


Figure 8: The efficiency coefficient  $\kappa$  as a function of the wall velocity  $\xi_w$  for fixed  $\alpha_N$ . The dashed and dashed-dotted lines mark the transitions from deflagrations to hybrids and further to detonations. The dashed-dotted line corresponds to Jouguet detonations (the only case used in the literature, although with a missing  $1/\xi_w^3$  factor). Analytical fits for  $\kappa(\alpha_N, \xi_w)$  are provided in Appendix A.

velocity  $\xi_w$  and the parameter  $\alpha_+$  (or  $\alpha_N$ ) the velocity profile is determined and  $\kappa$  can be calculated using eq. (30) independently from further assumptions on friction and microscopic physics in the plasma close to the wall (which are relevant to fix  $\xi_w$ ).

The results are shown in Fig. 8 which gives  $\kappa$  as a function of the wall velocity for several values of the vacuum energy  $\alpha_N$ . Note also that for large values of  $\alpha_N$ , small wall velocities are impossible, see Fig. 7 and the discussion about deflagrations in Sec. 3. The efficiency increases with  $\alpha_N$  and is maximal for the hybrid solutions. Nevertheless, according to numerical simulations, the detonation solutions are the only supersonic modes that are globally stable for small values of  $\alpha_N$  and realistically the maximal efficiency corresponds to the Jouguet case in this regime. The gravity wave literature focused on the Jouguet detonations (dashed-dotted line) and hence overestimated the efficiency  $\kappa$ . However, we stress that this effect is mostly compensated by the missing factor  $\xi_w^3$  in the formula of  $\kappa(\alpha)$  we mentioned before. In appendix A, we give fits to the efficiency  $\kappa$  shown in Fig. 8 as a function of the parameters  $\alpha_N$  and  $\xi_w$ .

Finally, it is interesting to estimate the thickness of the plasma shell near the bubble wall where the kinetic energy in the plasma is concentrated (as this is relevant for GW production). In Fig. 9 we give the thickness  $\Delta\xi$  of a shell around the transition wall such that it contains a given fraction of the kinetic energy,  $\Delta\kappa/\kappa$ , as indicated. For each type of bubble we choose the shell so as to maximize that fraction. That is, for detonations the shell is  $(\xi_w, \xi_w - \Delta\xi_w)$ ; for deflagrations  $(\xi_w - \Delta\xi_w, \xi_w)$  and in-between for hybrids. The dots in each line mark the boundaries between different regimes (deflagrations, hybrids and detonations, in order of increasing wall velocity). We see that, especially for hybrid solutions,

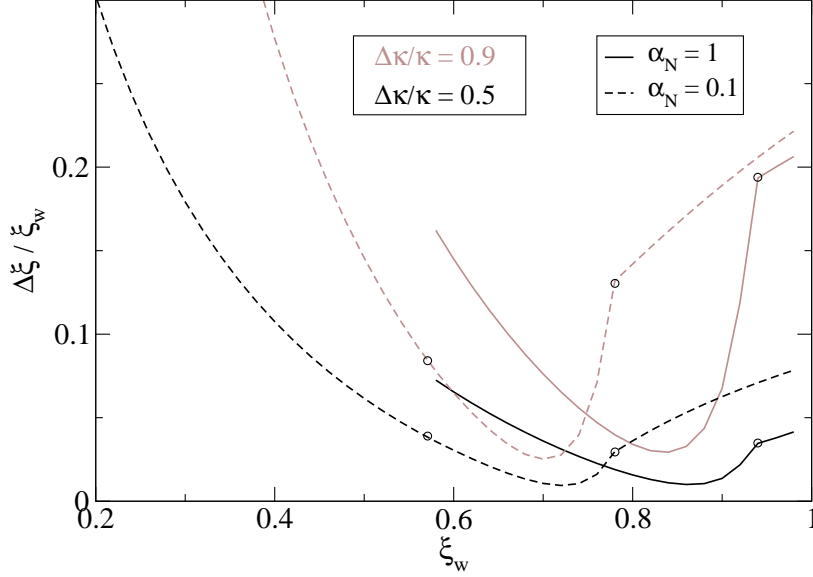


Figure 9: Curves with a fixed fraction of kinetic energy  $\Delta\kappa/\kappa$  in a shell of thickness  $\Delta\xi$  for  $\alpha_N = 0.1$  and  $\alpha_N = 1$  as a function of the wall velocity  $\xi_w$ . The lower black (upper brown) lines denote  $\Delta\kappa/\kappa = 0.5$  ( $\Delta\kappa/\kappa = 0.9$ ). The dots in each line mark the boundaries between different regimes (deflagrations, hybrids and detonations, in order of increasing wall velocity).

the kinetic energy is localized in the shock, which can be rather thin in this case. For weaker deflagrations, the shock is thicker. For detonations, part of the kinetic energy is always in the tail of the rarefaction wave.

In the limit of ultra-relativistic wall velocities ( $\xi_w \rightarrow 1$ ) the velocities  $v_{\pm}$  approach 1 with a relative slope  $v_+/v_-$  that depends on  $\alpha_+$  (see Fig. 1). Generically, the fluid velocity will not be ultra-relativistic in the plasma frame and the bubbles will expand as detonations (see Fig. 2). Expanding (21) in powers of  $1/\gamma_{\pm}$  one gets

$$\frac{\gamma_+^2}{\gamma_-^2} = 1 + 3\alpha_N, \quad v(\xi_w) = \mu(v_+, v_-) = \frac{3\alpha_N}{2 + 3\alpha_N}, \quad (41)$$

where we have used  $\alpha_+ = \alpha_N$  as we are in the regime of detonations. This relativistic case requires  $r = 1/(1 + 3\alpha_+)$ , which translates into  $p_+ - p_- = 2\epsilon$ . Numerically, the resulting efficiency in this limit is given by

$$\kappa \simeq \frac{\alpha_N}{0.73 + 0.083\sqrt{\alpha_N} + \alpha_N} \quad (\text{relativistic } \xi_w). \quad (42)$$

This result is relevant for the analysis of the case of runaway walls in section 6.

## 5 Bubble wall velocity for steady state walls

When a bubble of the broken phase is nucleated, and is large enough to start growing, it will expand in an accelerated way, with the difference in free-energy across its wall acting as

driving force. There is however a resistance to this expansion from the surrounding plasma, which exerts a friction force that grows with the velocity of the moving wall. Eventually, an equilibrium between these two forces is reached after a short time of expansion and, since then on, the bubble wall keeps expanding in a steady state at a constant terminal velocity. As explained in the last sections, hydrodynamics alone cannot be used to determine this terminal wall velocity and one has to analyze the mechanism of entropy production and friction in the wall.

## 5.1 EoM for the Higgs field and the friction parameter $\eta$

We take into account entropy production and friction through the equation of motion of the Higgs field

$$\square\phi + \frac{\partial V_0}{\partial\phi} + \sum_i \frac{dm_i^2}{d\phi} \int \frac{d^3p}{(2\pi)^3 2E_i} f_i(p) = 0 . \quad (43)$$

By decomposing

$$f_i(p) = f_i^{eq}(p) + \delta f_i(p) , \quad (44)$$

where  $f_i^{eq} = 1/[\exp(E_i/T) \mp 1]$  is the equilibrium distribution function of particle species  $i$  with  $E_i^2 = p^2 + m_i^2$ , eq. (43) takes the simple form (see also ref. [16] and more recently ref. [26])

$$\square\phi + \frac{\partial\mathcal{F}}{\partial\phi} - \mathcal{K}(\phi) = 0 , \quad (45)$$

where the second term gives the force driving the wall and  $\mathcal{K}(\phi)$  stands for the friction term

$$\mathcal{K}(\phi) = - \sum_i \frac{dm_i^2}{d\phi} \int \frac{d^3p}{(2\pi)^3 2E_i} \delta f_i(p) . \quad (46)$$

Friction is therefore due to deviations of particle distributions from equilibrium. In principle, calculation of  $\mathcal{K}(\phi)$  requires solving a coupled system involving Boltzmann equations for particle species with a large coupling to the Higgs field. This intricate calculation has been performed in the Standard Model [15] and in the MSSM [20] and under the assumption that the deviation from thermal equilibrium is small, i.e.  $\delta f_i(p) \ll f_i(p)$ , which is only true for weakly first-order phase transitions.

In this paper, we want to follow a more phenomenological and model-independent approach. In refs. [16, 26] a particularly simple choice for  $\mathcal{K}(\phi)$  was used:

$$\mathcal{K}(\phi) = T_N \tilde{\eta} u^\mu \partial_\mu \phi , \quad (47)$$

(where  $T_N$  is inserted just to make  $\tilde{\eta}$  dimensionless). This Lorentz invariant choice is motivated by similar approaches in the inflationary context but, as we will see in the next section, it does not lead to the correct behavior for highly relativistic bubble wall velocities: this friction force could increase without bounds, due to the  $\gamma$  factor appearing through  $u^\mu \partial_\mu \phi$ , but we know from ref. [27] that at large wall velocities the friction term approaches a constant (see next section).

Friction comes from out-of-equilibrium effects and the assumption that it depends locally only on the plasma four-vector  $u^\mu$  and a Lorentz scalar  $\eta$  is too simplistic. In our

phenomenological approach we ensure that the friction force grows with  $v$  and not  $\gamma v$ . Such behavior could arise from a friction term in the Higgs equation of motion of the form

$$\mathcal{K}(\phi) = T_N \tilde{\eta} \frac{u^\mu \partial_\mu \phi}{\sqrt{1 + (\lambda_\mu u^\mu)^2}} , \quad (48)$$

where the Higgs background is parametrized by a four-vector  $\lambda^\mu$  [such that  $\phi(\lambda^\mu x_\mu)$  and  $\lambda^\mu$  is  $(0, 0, 0, 1)$  in the wall frame]. One can show that the entropy production from such a term is always positive, as it should be.

Assuming then that in the steady state the bubble is large enough so that we can use the planar limit, using (48) in eq. (45) we get, in the wall frame,

$$\partial_z^2 \phi - \frac{\partial \mathcal{F}}{\partial \phi} = -T_N \tilde{\eta} v \partial_z \phi , \quad (49)$$

where  $z$  is the direction of the wall velocity. Note that the right-hand side would be multiplied by  $\gamma$  if we use (47) instead of (48). If we multiply this differential equation by  $\partial_z \phi$  on both sides and integrate across the wall, we get

$$\int dz \partial_z \phi \frac{\partial \mathcal{F}}{\partial \phi} = T_N \tilde{\eta} \int dz v (\partial_z \phi)^2 . \quad (50)$$

The integration of the force term could be simply performed if the free energy  $\mathcal{F}$  did not have an implicit dependence on  $z$  via the change in the temperature,  $T(z)$ , with  $T(\pm\infty) = T_\pm$ . Using  $d\mathcal{F}/dz = (\partial\mathcal{F}/\partial\phi)\partial_z\phi + (\partial\mathcal{F}/\partial T)\partial_z T$ , one can rewrite the driving force of the bubble expansion as:

$$F_{dr} \equiv \int dz \partial_z \phi \frac{\partial \mathcal{F}}{\partial \phi} = \mathcal{F}|_-^+ - \int dz \partial_z T \frac{\partial \mathcal{F}}{\partial T} , \quad (51)$$

and, using  $\epsilon_\pm$  and  $a(z)$  as defined in eqs. (16) and (17), one gets, without making assumptions on the plasma equation of state:

$$F_{dr} = \epsilon_+ - \epsilon_- - \frac{1}{3} \int da T^4 . \quad (52)$$

By making further use of the definition of  $a(z)$  and assuming that the distribution functions for particle species are the equilibrium ones one can rewrite eq. (52) as

$$F_{dr} = \Delta V_0 + \sum_i |N_i| \int dz \frac{dm_i^2}{dz} \int \frac{d^3 p}{(2\pi)^3} \frac{f_i^{eq}}{2E_i} , \quad (53)$$

where  $\Delta V_0$  is the  $T = 0$  part of  $\epsilon_+ - \epsilon_-$ , that is, the difference in  $(T = 0)$  potential energy between the symmetric and broken minima ( $\epsilon$ , for the bag equation of state). This expression for the driving force will be useful in sect. 6.

Notice that this force does not coincide with the latent heat  $\Lambda$ , given by

$$\Lambda \equiv e_+ - e_- = \left( \epsilon + a T^4 \right) \Big|_-^+ . \quad (54)$$

nor with the free energy (pressure) difference

$$\Delta \mathcal{F} \equiv p_- - p_+ = \left( \epsilon - \frac{a}{3} T^4 \right) \Big|_-^+ . \quad (55)$$

Using the fact that the number of effective degrees of freedom decreases continuously in the wall, the last integral in (52) is bounded as

$$\frac{1}{3}(a_+ - a_-)T_{min}^4 \leq \frac{1}{3} \int da T^4 \leq \frac{1}{3}(a_+ - a_-)T_{max}^4, \quad (56)$$

where  $T_{min} = \text{Min}\{T_-, T_+\}$  and  $T_{max} = \text{Max}\{T_-, T_+\}$ . For weak phase transitions one typically has  $T_+ \approx T_-$  and the concrete choice of the profiles in the wall are not important. For very strong phase transitions, the free energy is dominated by the vacuum contribution and the plasma contribution is rather small altogether:

$$F_{dr} \approx \Delta\mathcal{F} \approx \epsilon_+ - \epsilon_- - (a_+ - a_-)\frac{T^4}{3} \quad (\text{for weak phase transitions}) \quad (57)$$

$$F_{dr} \approx \Delta\mathcal{F} \approx \Lambda \approx \epsilon_+ - \epsilon_- \quad (\text{for strong phase transitions}) \quad (58)$$

For simplicity, let us approximate the integral in eq. (56) by the expression involving  $T_+$ . For other approximations the results would not change qualitatively. In this case, the Higgs equation of motion gives

$$\alpha_+ - \frac{1}{3} \left(1 - \frac{a_-}{a_+}\right) = \frac{\tilde{\eta}T_N}{a_+T_+^4} \int dz v (\partial_z \phi)^2. \quad (59)$$

In the SM, the second term in (59) is roughly  $(1 - a_-/a_+)/3 = 0.05$ . For small values of  $\alpha_+$  the left hand side of (59) is negative and no bubbles can nucleate (for nucleation one can consider  $T_+ = T_-$ , in which case  $F_{dr} = \mathcal{F}_+ - \mathcal{F}_-$ , so that the wrong sign of the free-energy difference is the reason that prevents the phase transition). For larger values of  $\alpha_+$ , the left-hand side of the equation is positive and has to be balanced by the friction force so as to obtain a constant wall velocity, as already explained. We will rewrite the right hand side of (59) as

$$\frac{\tilde{\eta}T_N}{a_+T_+^4} \int dz v (\partial_z \phi)^2 \equiv \eta \frac{\alpha_+}{\alpha_N} \langle v \rangle, \quad (60)$$

which serves as the definition of  $\eta$ . Here  $\langle v \rangle$  denotes the fluid velocity average across the wall (in the wall frame), that we approximate as

$$\langle v \rangle \equiv \frac{\int dz v (\partial_z \phi)^2}{\int dz (\partial_z \phi)^2} \simeq \frac{1}{2}(v_+ + v_-). \quad (61)$$

In this way, (59) is simply written as<sup>4</sup>

$$\alpha_+ - \frac{1}{3} \left(1 - \frac{a_-}{a_+}\right) = \eta \frac{\alpha_+}{\alpha_N} \langle v \rangle. \quad (62)$$

Eq. (62) reproduces the correct behavior for small and very large wall velocities, even though the parameter  $\eta$  will not be the same in these two limits. This simple phenomenological approach already reproduces almost all qualitative features found in the hydrodynamic

---

<sup>4</sup>Compared to ref. [26], our velocity average does not include a  $\gamma$  factor and we use a different expression for the driving force.

simulations performed in ref. [16]. Notice that the right hand side of (59) is an increasing function of the wall velocity (since  $v_+$  and  $v_-$  are, see also Fig. 6). On the other hand, the left hand side of the equation is decreasing for small velocities and jumps when the flow solutions change from deflagrations to detonations (also the velocity  $v_+$  jumps but this is less essential). Hence, for a certain range of values of the friction coefficient  $\eta$ , eq. (59) has two solutions while in ref. [16] three solutions were found. The discrepancy is due to the fact that we neglect the thickness of the wall compared to the shock and this would smooth out the jumps in  $v_+$  and  $\alpha_+/\alpha_N$ , thus producing a third solution. The three solutions would in the present model then be a deflagration (or a hybrid solution), a weak detonation and a configuration close to a Jouguet detonation, in agreement with the results found in ref. [16].

Finally, at the critical temperature at which the two phases have degenerate free energy, one expects that the gravitational wave signal vanishes. However, an analysis using the Jouguet condition still implies supersonic bubble expansion. This led to the fact that the difference in free energy is often confused with the vacuum energy  $\epsilon$  in the literature on gravitational wave production that is based on the Jouguet condition. Replacing the Jouguet condition by the equation of motion (EoM) of the Higgs field solves this problem consistently, since at the critical temperature one obtains  $\alpha_N = (1 - a_-/a_+)/3$  and, according to equation (62), the bubble cannot expand.

## 5.2 Wall velocity in the $(\eta, \alpha_N)$ plane

A fully numerical calculation of  $\langle v \rangle$  in a given model would require the following procedure. The starting point is the computation of the free-energy (in some approximation) as a function of the Higgs field and the temperature,  $\mathcal{F}(\phi, T) = -p$ . First, the nucleation temperature  $T_N$  of the phase transition should be determined (this is standard). To obtain the steady-state profiles across the phase-transition wall in the planar limit of quantities like the velocity, temperature and Higgs field, one should integrate the following system of coupled differential equations:

$$\begin{aligned} \partial_z^2 \phi - \frac{\partial \mathcal{F}}{\partial \phi} + T_N \tilde{\eta} v \partial_z \phi &= 0 , \\ \partial_z [\omega \gamma^2 v] &= 0 , \\ \partial_z \left[ \frac{1}{2} (\partial_z \phi)^2 + \omega \gamma^2 v^2 + p \right] &= 0 . \end{aligned} \tag{63}$$

In addition to the first Higgs equation which we already discussed, the two extra equations correspond to the differential (and static) form of energy-momentum conservation. Their integration across the wall gives immediately the Steinhardt's matching conditions (9).

One wants to solve the system (63) for the primary quantities  $\phi(z)$ ,  $T(z)$  and  $v(z)$ . The boundary conditions for  $\phi(z)$  are

$$\phi(-\infty) = \phi_0(T_-) \quad \text{and} \quad \phi(\infty) = 0, \tag{64}$$

where  $\phi_0(T_-)$  is the Higgs vacuum expectation value in the broken phase at some temperature  $T_-$  to be determined. The  $z = \pm\infty$  boundaries correspond to the assumption that the width of the phase transition front is much smaller than the width of the shell with non-zero

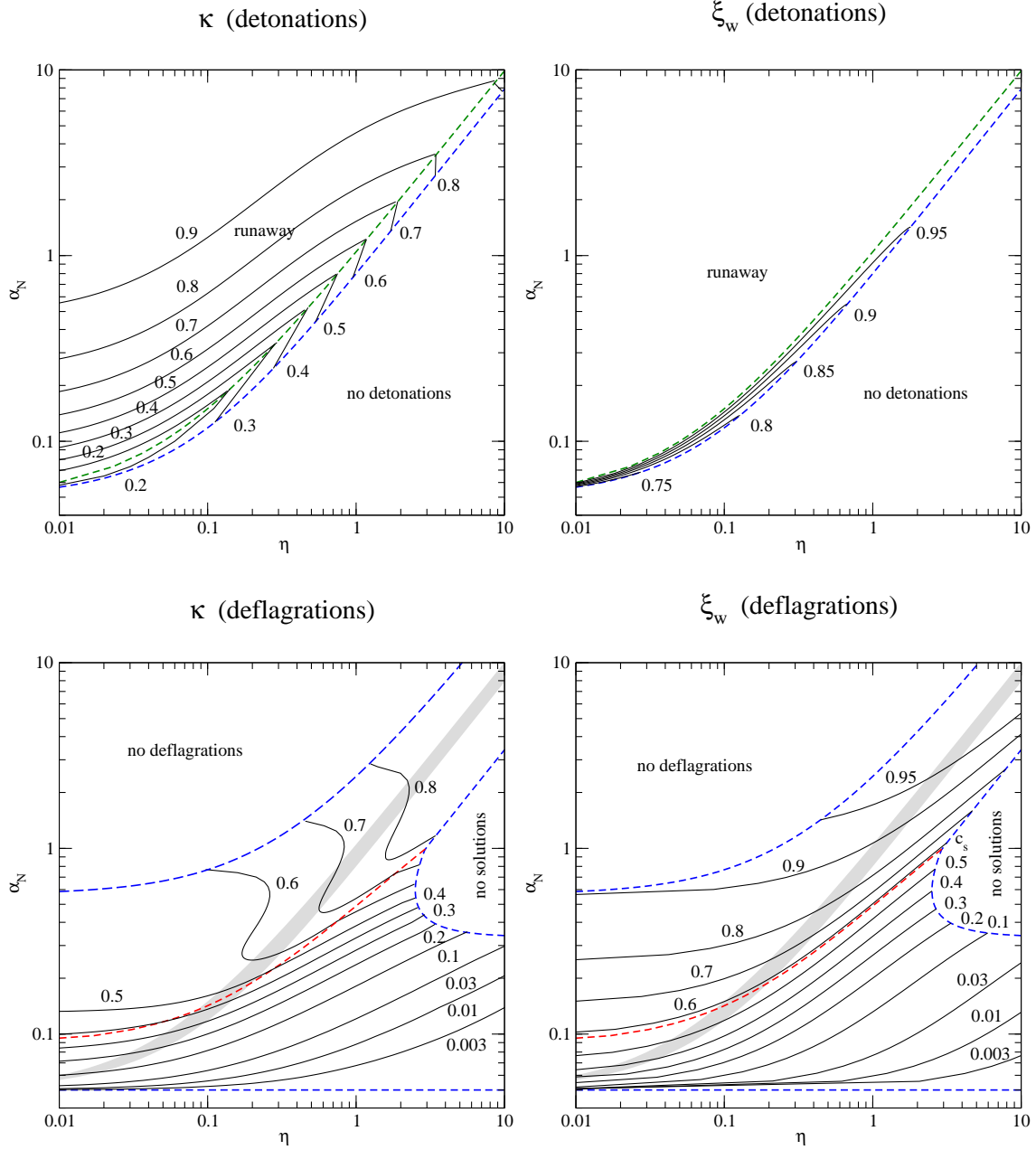


Figure 10: Contour plots of  $\kappa$  and  $\xi_w$  as functions of  $\eta$  and  $\alpha_N$  (for  $a_-/a_+ = 0.85$ ). The blue lines mark the transition to regions without solutions. The green lines mark the boundaries between stationary and runaway solutions. The red lines mark the transition from subsonic to supersonic deflagrations (hybrids). We superimposed the detonation region in the lower plots as a gray band.

plasma velocity, which in general is a very good approximation. For  $\tilde{\eta}$  fixed, the boundary conditions (say at  $z = -\infty$ ) for  $T(z)$  and  $v(z)$  cannot be chosen freely: e.g. if one fixes  $T(+\infty) = T_+$  (in general different from  $T_N$ ) only one particular  $v(+\infty) = v_+$  is selected and then all profiles  $\phi(z)$ ,  $T(z)$ ,  $v(z)$  can be determined. Detonation solutions will have  $v(+\infty) = v_+ = \xi_w > v(-\infty) = v_-$  and one should choose  $T(+\infty) = T_N$ . Deflagrations

will have instead  $v_+ < v_- = \xi_w$  and  $T(+\infty) = T_+$  has to be set consistently with such wall velocity (and corresponding deflagration hydrodynamic profile). Finally, hybrid solutions have  $v_+ < v_- = c_s^-$ . Their wall velocity,  $\xi_w > c_s^-$  is not fixed unequivocally by  $v_\pm$  but should match the choice of  $T_+$ . Our analytical formula (62) is expected to give a reasonable approximation to the more complicated numerical approach just described. Such simple formula is very useful to investigate in a model-independent way the parametric dependences of the wall velocity (and derived quantities) in different regimes of bubble expansion, which we do next.

Armed with eq. (62) we can calculate the wall velocity for given values of  $\alpha_N$  (that measures the strength of the transition) and  $\eta$  (that measures the friction of the plasma). The results are shown in Fig. 10, which plots contour lines of the wall velocity  $\xi_w$  and the efficiency coefficient  $\kappa$  in the plane  $(\eta, \alpha_N)$ , for the particular case of  $a_-/a_+ = 0.85$  (as in the SM). Let us first explain the different boundaries of the parameter space available in the plane  $(\eta, \alpha_N)$ . For the bubbles to be able to grow, the left hand side of (62) should be positive. This requires  $\alpha_+ > (1 - a_-/a_+)/3$  which, in this particular example, gives  $\alpha_N \geq \alpha_+ > 0.05$ . Both the low horizontal boundary ( $\alpha_N > 0.05$ ) and the boundary at larger  $\alpha_N$  and small  $\eta$  come from this requirement. That bubbles might not be able to grow even if the transition is in principle quite strong (large  $\alpha_N$ ) is due to the fact that one can have  $\alpha_+ \ll \alpha_N$  for hybrid solutions (see figs. 6 and 14). The boundary at  $\alpha_N > 1/3$  and large  $\eta$  corresponds to the extreme case with  $v_+ \rightarrow 0$  and  $T_- \rightarrow 0$  and determines the maximal possible value of the friction coefficient for a given  $\alpha_N$ . We have plotted separately the cases of detonations and deflagrations. Runaway solutions are realized for strong transitions and small friction as one would expect. We see that for weak phase transitions and small friction, deflagrations compete with detonations (superimposed in the lower plots as a gray band). In the overlapping region, the wall velocity for the deflagration solution is always smaller than for the detonation solution, which could have indicated that the deflagration solution is reached first and is therefore realized. However, hydrodynamic simulations indicate that these solutions turn out to be unstable globally and in this regime the phase transition proceeds by detonation bubbles [19] (or eventually by runaway behavior if the upper bound on friction would be incorporated in the model). Henceforth, the only way of realizing supersonic deflagrations is in a regime where hybrids but no detonations are possible [19].

### 5.3 Microscopic determination of $\eta$

In the following we provide the connection of our results to the work [15, 20] in which the friction in the wall was explicitly calculated in the SM and MSSM<sup>5</sup>. The friction force in ref. [20] is of the form

$$F_{fr} = \hat{\eta} \langle v \rangle T_N \int dz \phi^2 (\partial_z \phi)^2, \quad (65)$$

where  $\hat{\eta}$  is a constant that depends mostly on the particle content of the model and its couplings to the Higgs.  $\phi(z) = \frac{1}{2}\phi_N[1 + \tanh(z/l_w)]$  where  $l_w$  is the wall thickness and  $\phi_N$  is the Higgs vev at nucleation temperature. Comparison with our friction force shows that

---

<sup>5</sup>We consider those results more reliable than the ones of refs. [28, 26] which deduce particle distribution functions  $\delta f$  without taking interactions into account.



our parameter  $\eta$  can be written as

$$\eta \sim \frac{\hat{\eta}}{10 a_+} \frac{1}{T_N l_w} \left( \frac{\phi_N}{T_N} \right)^4 \quad (66)$$

The coefficient  $\hat{\eta}$  was determined in the SM [15] ( $\hat{\eta} \approx 3$ ) and in the MSSM [20] ( $\hat{\eta} \lesssim 100$  with a sizable dependence on  $\tan \beta$ ). A particularly interesting case is given by the parameter region of the MSSM that allows for viable electroweak baryogenesis. The bound on sphaleron wash-out implies  $\phi_N/T_N \gtrsim 1$  and using  $T_N l_w \approx 10$ ,  $\hat{\eta} \approx 100$  one finds  $\eta \approx 1/30$ . Due to a small difference in free energies, this leads to subsonic wall velocities  $\langle v \rangle = 0.05 \div 0.1$  [20] as required for the diffusion of CP-violating particle densities into the symmetric phase in front of the wall. This corresponds to a very weak phase transition with a value of  $\alpha_N$  just slightly above its lower bound (that depends on  $a_-/a_+$ ). Note that for models with a similar particle content the friction  $\eta$  is not expected to change much, while the strength of the phase transition can increase significantly. This is for example the case in singlet extensions of the SM and MSSM which can easily lead to detonations or runaway solutions.

In this section we have assumed that the bubble wall reaches at some (not too late) stage of the expansion a constant velocity. In this case the fraction of energy transformed into kinetic energy of the Higgs field becomes negligible, since it only scales with the surface of the bubble, while the similarity solutions of bulk motion scale with the volume. This can change in cases in which the wall keeps accelerating without reaching a terminal velocity, as discussed in the next section.

## 6 Runaway walls

It was recently argued [27] that the friction exerted on the Higgs wall by the plasma might be too small and the wall might continuously accelerate. In this case a constant fraction of the free vacuum energy is transformed into kinetic and gradient energies of the wall. In this section we analyze the energy balance and the efficiency coefficient in this situation.

Let us first quickly present the main result of [27] that is based on the analysis of refs. [29–31]. The passing phase-transition wall disturbs the distribution functions of particles in the plasma. As discussed in the previous section, if we knew such non-equilibrium distributions,  $f_i(p, z)$ , for each particle species, we could write, for the total force acting on the wall per unit area and including friction:

$$F_{tot} = F_{dr} - F_{fr} = \Delta V_0 + \sum_i |N_i| \int dz \frac{dm_i^2}{dz} \int \frac{d^3 p}{(2\pi)^3} \frac{f_i}{2E_i}. \quad (67)$$

This has the same form as eq. (53) for the driving force  $F_{dr}$  but with the replacement  $f_i^{eq} \rightarrow f_i$ . Now, the ultra-relativistic case is particularly simple: to leading order in  $1/\gamma_w$ , the wall induces a sudden change in particle masses,  $m_{i,+}^2 \rightarrow m_{i,-}^2$ , but leaves particle distribution functions as they were in the symmetric phase  $f_i = f_{i,+}^{eq}$  (which are not the equilibrium ones in the broken phase). This allows the  $z$ -integral in (67) to be performed and one obtains

$$F_{tot} = \Delta V_0 - \sum_i |N_i| \Delta m_i^2 \int \frac{d^3 p}{(2\pi)^3} \frac{f_{i,+}^{eq}}{2E_{i,+}}, \quad (68)$$

where  $\Delta m_i^2 = m_i^2|_+^-$  and  $E_{i,+}$  in the momentum integral is also the one corresponding to the symmetric phase, as indicated.

If  $F_{tot}$  remains positive even for  $v \rightarrow 1$ , the system will enter the runaway regime. Besides the explicit form (68), this condition can be rephrased in terms of the free energies in the mean field approximation [27]. Notice that the mean field approximation implies

$$\langle V_T(\phi) \rangle_{MF} = V_T(0) + \sum_i [m_i^2(\phi) - m_i^2(0)] \left. \frac{dV_T}{dm_i^2} \right|_0, \quad (69)$$

such that

$$\langle V_T^- \rangle_{MF} = \langle V_T^+ \rangle_{MF} + \sum_i \Delta m_i^2 \left. \frac{dV_T}{dm_i^2} \right|_+, \quad (70)$$

and the criterion for runaway behaviour reads

$$0 < F_{tot} = \langle \mathcal{F}^+ - \mathcal{F}^- \rangle_{MF}. \quad (71)$$

The results we just summarized can be interpreted as saying that the friction  $F_{fr}$  (which we expect to increase monotonically with  $v$ ) saturates at a finite value<sup>6</sup> for  $v \rightarrow 1$ . A sketch for this behavior is given in Fig. 11. Noting that the driving force is given by

$$F_{dr} = \mathcal{F}^- - \mathcal{F}^+, \quad (72)$$

then the maximal value for the friction force reads ( $\langle \mathcal{F}^+ \rangle_{MF} = \mathcal{F}^+$ )

$$F_{fr}^{max} = \langle \mathcal{F}^- \rangle_{MF} - \mathcal{F}^- = \langle V_T^- \rangle_{MF} - V_T^- \quad (73)$$

Using the convexity properties of the different contributions to  $V_T$  one can show that  $F_{fr}^{max}$  is necessarily positive.

If  $\langle \mathcal{F}^+ - \mathcal{F}^- \rangle_{MF} > 0$ , then  $F_{dr} < F_{fr}^{max}$ , and the wall velocity will grow till the friction force equilibrates  $F_{dr}$  and a steady state with some terminal velocity is reached. In the opposite case with  $\langle \mathcal{F}^+ - \mathcal{F}^- \rangle_{MF} < 0$ , one has  $F_{dr} > F_{fr}^{max}$  and the wall will keep accelerating without reaching a steady state, i.e. it will “run-away”. The crucial assumptions here are that there are no hydrodynamic obstacles that prohibit the wall velocities to become highly relativistic in the first place, and that the mean free-path of the particles is larger than the wall thickness.

It is instructive to rederive the results of ref. [27] we have just presented in the language of Kadanoff-Baym equations (see refs. [32] for an introduction to Kadanoff-Baym equations in Wigner space). In this formalism, the Wightman function  $G_i^<$  (for particle species  $i$ ) is the relevant Green function that encodes the distribution function of the particles in the plasma. Under the assumption that the mean free-path of the particles that obtain a mass by the Higgs vacuum expectation value is much larger than the thickness of the bubble wall, one can neglect collisions in the wall. In this case the Kadanoff-Baym equation for the Wightman function  $G_i^<$  reads

$$(p^2 - m_i^2) e^{i\phi/2} G^< = 0, \quad (74)$$

---

<sup>6</sup>Up to a possible logarithmic increase with  $\log \gamma_w$  (we thank Guy Moore for clarifications on this point).

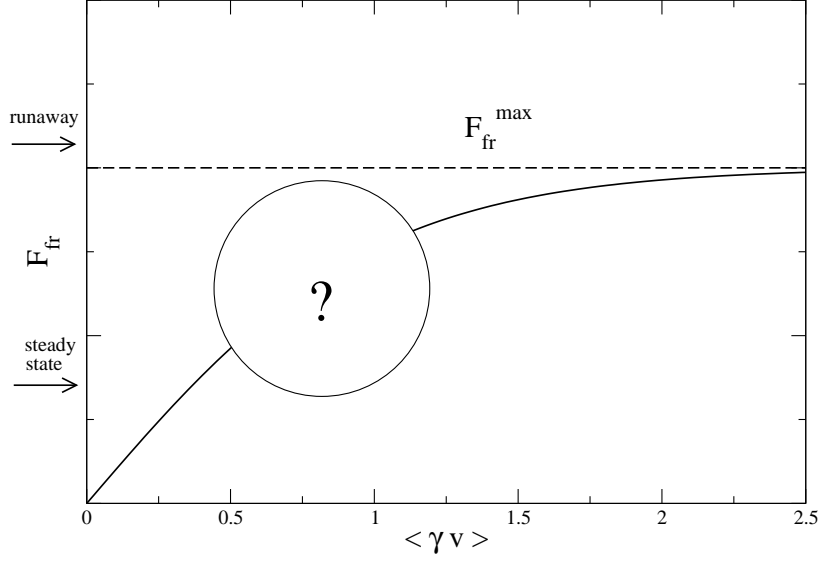


Figure 11: A sketch of the friction force as a function of the wall velocity showing the saturation at  $\langle v \rangle \rightarrow 1$ . The behavior for intermediate velocities is largely unknown. The arrows indicate two possible values for the driving force that would lead to steady or runaway bubble expansion, as indicated.

where the diamond operator is defined as

$$\diamond = \overleftarrow{\partial}_x \overrightarrow{\partial}_p - \overleftarrow{\partial}_p \overrightarrow{\partial}_x. \quad (75)$$

In the semi-classical limit, the operator  $e^{i\phi/2}$  can be expanded in gradients and the real/imaginary parts of the equations become, at first order,

$$(p^2 - m_i^2)G_i^< = 0, \quad (76)$$

$$(p^2 - m_i^2) \diamond G_i^< = 0. \quad (77)$$

The gradient expansion is justified in the present case because in the wall frame the particles have momenta of order  $\gamma T$ , which is large compared to the inverse wall thickness. Using the ansatz

$$G_i^< = 4\pi \delta(p^2 - m_i^2) f_i(x^\mu, p^\mu), \quad (78)$$

this yields for the particle distribution function the equation

$$\left[ p \cdot \partial_x + \frac{1}{2} (\partial_\zeta m_i^2) \lambda \cdot \partial_p \right] f_i(x^\mu, p^\mu) = 0. \quad (79)$$

We introduced again a four-vector  $\lambda_\mu$  to parametrize the motion of the wall [that is,  $\lambda_\mu = (0, 0, 0, 1)$  in the frame moving with the wall] and  $\zeta \equiv \lambda \cdot x$ . Notice that the first term in (79) is the flow term of a Boltzmann equation while the second term represents the force from the wall acting on the plasma. In front of the wall the distribution function is given by the equilibrium one. E.g., for a bosonic degree of freedom

$$f_{i,+}^{eq} = \frac{\theta(p_0)}{\exp[\beta(u \cdot p)] - 1}, \quad (80)$$

where  $u^\mu$  is the plasma velocity four-vector. Solving eq. (79) the distribution function behind the wall reads (with  $\Delta m_i^2$  as before)

$$f_i = \frac{\theta(p_0)}{\exp \beta \Omega_i - 1}, \quad (81)$$

with

$$\Omega_i = u \cdot p + u \cdot \lambda \left[ \lambda \cdot p - \text{sign}(\lambda \cdot p) \sqrt{(\lambda \cdot p)^2 + \Delta m_i^2} \right]. \quad (82)$$

In the wall frame this yields

$$\Omega_i = \gamma p_0 - \gamma v \sqrt{p_z^2 + \Delta m_i^2}. \quad (83)$$

This is in accord with the results of [27] and our previous discussion: in the wall frame the particles just cross the wall and change their momentum according to

$$p_z^2 \rightarrow p_z^2 - \Delta m_i^2. \quad (84)$$

The contribution of particle species  $i$  to the pressure behind the wall is (in the wall frame and per degree of freedom) given by

$$\begin{aligned} \delta_i T_{zz}^{plasma} &= \int \frac{d^4 p}{(2\pi)^4} p_z^2 G_i^< \\ &= 2 \int \frac{d^4 p}{(2\pi)^3} \delta(p^2 - m_{i,-}^2) p_z^2 f_i \\ &\approx 2 \int \frac{d^4 p}{(2\pi)^3} \delta(p^2 - m_{i,+}^2) p_z \sqrt{p_z^2 - \Delta m_i^2} \text{sign}(p_z) \theta(p_z^2 - \Delta m_i^2) f_{i,+}^{eq}, \end{aligned} \quad (85)$$

where the last line is obtained by shifting the integration variable as in (84) and noting that the measure  $dp_z p_z$  does not change. Hence, for the pressure difference produced by the plasma this gives

$$\begin{aligned} \delta_i \Delta T_{zz} &\approx \Delta m_i^2 \int \frac{d^4 p}{(2\pi)^3} \delta(p^2 - m_{i,+}^2) f_{i,+}^{eq} \\ &= \Delta m_i^2 \int \frac{d^3 p}{(2\pi)^3 2E} f_{i,+}^{eq}, \end{aligned} \quad (86)$$

which agrees with the formula obtained in ref. [27]. In terms of  $\Delta T_{zz}$ , the criterion for runaway solutions is very transparent and is simply

$$\epsilon > \Delta T_{zz} = \sum_i \delta_i \Delta T_{zz}. \quad (87)$$

In this case, only a part of the available vacuum energy is released into the plasma and the remaining energy is used to further accelerate the wall.

This criterion for runaway behavior can be reformulated in terms of parameters of the phase transition in case it is rather strong. For particles that are light in both phases, the

contribution to the pressure is similar in both phases. Particles that are heavy in both phases do not contribute much to either pressure difference or free energy. Hence, mostly the particles that become heavy during the phase transition produce a pressure difference along the wall. Using this, one obtains for an accelerated wall the criterion

$$\Delta T_{zz} = \frac{T_N^2}{24} \sum_{light \rightarrow heavy} c_i |N_i| m_i^2 = \frac{T_N^2}{24} \langle \phi \rangle^2 \sum_{light \rightarrow heavy} c_i |N_i| y_i^2 < \epsilon, \quad (88)$$

with  $c_i = 1$  ( $1/2$ ) for bosons (fermions),  $|N_i|$  are the corresponding numbers of degrees of freedom,  $y_i$  are the coupling strengths to the Higgs boson and  $\langle \phi \rangle$  the Higgs vacuum expectation value in the broken phase. Using the relation  $\epsilon = \alpha_N (a_N T_N^4)$  we get that a runaway wall is in principle possible for

$$\alpha_N > \alpha_\infty \equiv \frac{30}{\pi^2} \left( \frac{\langle \phi \rangle}{T_N} \right)^2 \frac{\sum_{light \rightarrow heavy} c_i |N_i| y_i^2}{\sum_{light} c'_i |N_i|}, \quad (89)$$

with  $c'_i = 1$  ( $7/8$ ) for bosons (fermions). This equation serves as the definition of  $\alpha_\infty$ . In extensions of the SM, eventually more particles contribute to the pressure difference, but typically not many new light particles are in thermal equilibrium. One hence can deduce that for

$$\alpha_N > 1.5 \times 10^{-2} \left( \frac{\langle \phi \rangle}{T_N} \right)^2, \quad (90)$$

runaway walls are possible depending on the details of the model. It is interesting to note that models which lead to sizable gravitational wave production typically satisfy the runaway condition and this should be taken into account when calculating the GW signal.

Next, we make contact with the case of a constant wall velocity, discussed in the last section.

## 7 Energy budget of first-order phase transitions

The analysis in the last section assumed that the system was time-independent in the wall frame, which leads to the fact that the Higgs field only contributes a pressure component from the vacuum energy to the energy momentum tensor

$$T_{zz}^\phi|_-^+ = -\epsilon, \quad T_{0z}^\phi|_-^+ = 0. \quad (91)$$

In a static system these contributions have to be compensated by the plasma and this requires

$$T_{zz}^{plasma}|_-^+ = \epsilon, \quad T_{0z}^{plasma}|_-^+ = 0. \quad (92)$$

Such relations lead to the matching conditions (9) used as boundary conditions in the hydrodynamic analysis of the plasma. In the case of a highly relativistic plasma, these boundary conditions can be derived explicitly from the particle distribution functions. Following the same calculation as in the previous section, for  $T_{0z}^{plasma}$  one finds

$$T_{zz}^{plasma}|_-^+ = \Delta T_{zz}, \quad T_{0z}^{plasma}|_-^+ = 0, \quad (93)$$

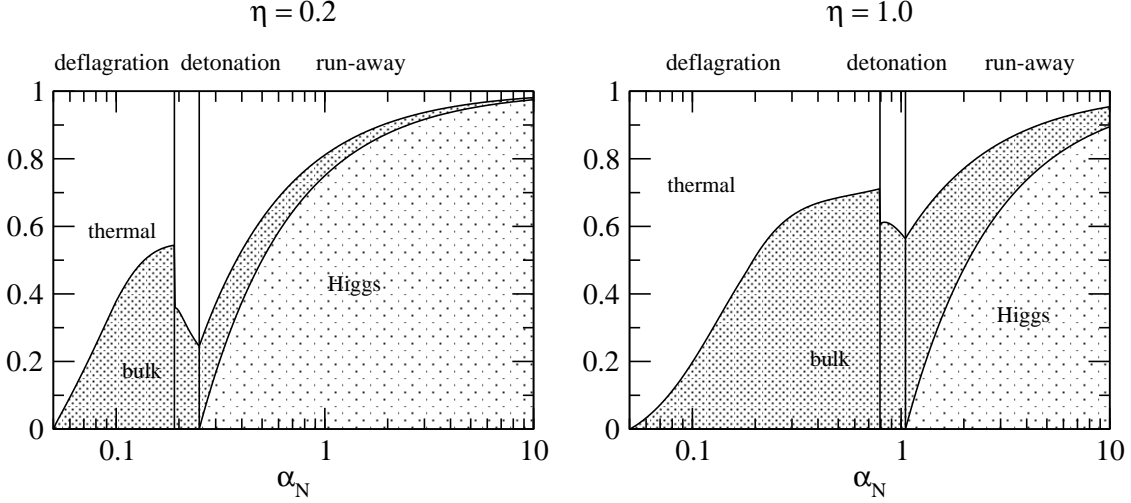


Figure 12: The energy budget for  $\eta = 0.2$  and  $\eta = 1.0$ . The different contributions (from top to bottom) are thermal energy, bulk fluid motion and energy in the Higgs field. The last two components can potentially produce anisotropic stress in the plasma and subsequently gravity waves.

Hence, in the runaway case, with  $\alpha_N > \alpha_\infty$  the solutions for the fluid motion are identical to the ones with  $\alpha_N = \alpha_\infty$ , according to the distribution functions determined close to the wall. At the same time the Higgs field cannot be time-independent anymore and energy momentum conservation implies that the remaining energy is used to accelerate the wall.

We observed in section 4 that, in the limit of large wall velocities, the efficiency factor does not depend on the wall velocity but is given by (42). This means that, in the runaway case,

$$\kappa_\infty \simeq \frac{\alpha_\infty}{0.73 + 0.083\sqrt{\alpha_\infty + \alpha_\infty}} \quad (\text{runaway}). \quad (94)$$

In summary, in the runaway regime and for given  $\alpha_N$ , a portion  $\alpha_\infty$  of the initial  $\alpha_N$  produces bulk motion with efficiency  $\kappa_\infty$ , as given by eq. (94), while the remaining portion,  $\alpha_N - \alpha_\infty$ , is transformed directly into kinetic/gradient energy of the Higgs field with efficiency  $\kappa = 1$ . These two components can potentially produce anisotropic stress in the plasma and subsequently gravity waves while the thermal energy in the plasma can not. Figure 12 shows the energy budget of the phase transition for two choices of the friction coefficient  $\eta$  as a function of  $\alpha_N$  in different regimes of bubble expansion.

## 8 Summary

The bubble wall velocity  $\xi_w$  in first-order phase transitions is a key quantity entering the calculation of the baryon asymmetry in electroweak baryogenesis and its derivation has been discussed extensively in the literature. However, it has been treated in detail only in specific models (corresponding to weak first-order phase transitions) and a general account of the problem was lacking. In this work, we attempted to gather all the important information in a self-consistent manner and in a model-independent approach. We presented a unified

description of all the different regimes characterizing bubble growth and stressed how they are connected.

In the last few years, there has been a significant effort towards working out the relic gravity wave background generated by bubble collisions. Production of gravity waves during a first-order phase transition is due to bulk motions in the plasma and magnetic fields generated by these fluid motions. The resulting gravity wave spectrum scales as a large power of the typical fluid velocity, roughly as  $v^4$ . The fluid velocity profile in the vicinity of the bubble wall is relevant and it is therefore important to estimate the fraction  $\kappa$  of the vacuum energy density  $\epsilon$  liberated during the phase transition which goes into the fluid motions.

So,  $\xi_w$  and  $\kappa$  are the two salient quantities that one would like to predict for any given particle physics model leading to a first-order phase transition. The most straightforward quantity to compute in a given model is  $\alpha_N$ , the ratio of the vacuum energy density  $\epsilon$  to the radiation energy density at the nucleation temperature. One would be interested in knowing in which regime (detonation, deflagration, hybrids, runaway) the given model is expected to fall in, without having to deal with the intricate Boltzmann equations. There is a relation which has been used extensively in the literature for  $\xi_w$  as a function of  $\alpha_N$ . Such relation is valid for supersonic walls and is based on the assumption of Jouguet detonations. Assuming Jouguet detonations amounts to setting the value of the fluid velocity at the inner boundary of the velocity profile in the wall frame to the speed of sound. There is no justification for this choice although it has been used in the literature for simplicity. Setting arbitrarily some boundary condition for the velocity leads to inconsistencies and corresponds to ignoring the constraints from the equation of motion of the Higgs field. By dealing explicitly with that Higgs equation, our study goes beyond this assumption.

The difficulty is that the problem under consideration is not fully determined by  $\alpha_N$ . As we elucidated, for a given  $\alpha_N$ , there are many possible wall velocities and a large range of  $\kappa$  values<sup>7</sup>, as seen in Fig. 8. To fix the solution, one needs to compute the friction term that restrains the bubble expansion. There are two approaches to this problem. The rigorous (but tedious) treatment requires solving coupled Boltzmann equations. A simpler approach is to take the friction as a parameter independent from the bubble wall velocity and solve the equation of motion for the Higgs field by using some phenomenological description for the friction. This is the approach that we took in this paper. It has been adopted in some numerical studies [14, 16–19], although the modeling of the friction was not appropriate in the limit of large velocities. We now use a more realistic modeling which allows us to describe the runaway regime in addition to the steady state regime, eq. (49).

One of our final results has been to present, in Fig. 10, model-independent contours for  $\xi_w$  and  $\kappa$  in the  $\eta - \alpha_N$  plane, where  $\eta$  and  $\alpha_N$  are the two crucial physical (dimensionless) parameters respectively characterizing the strength of the phase transition and the amount of friction. In concrete models,  $\alpha_N$  and  $\eta$  are not independent parameters. However, we believe that the information contained in these plots is useful as it enables to investigate the parametric dependence of the wall velocity and the  $\kappa$  factor in different regimes and gather all the important physics in a single comprehensive figure. The contour plots are not fully model-independent as we have fixed the relative change in the number of relativistic degrees

---

<sup>7</sup>We have also corrected a missing factor  $1/\xi_w^3$  in the definition of  $\kappa$  which is found in the literature.

of freedom between the two phases but they serve the purpose of describing the qualitative behavior of  $\xi_w$  and  $\kappa$ . From our analysis, we obtain that only a small band in the  $(\eta, \alpha_N)$  plane leads to pure detonations. We also find that in a large region of this plane, hybrids coexist with runaway solutions, meaning that our time-independent analysis is not sufficient to fix the solution. According to numerical studies, hybrids are mostly unstable [19]. We would therefore conclude that the most likely solutions are either deflagrations or runaway solutions. We have clarified the condition determining the runaway regime, see eq. (89), and found that for values  $\alpha_N \sim \mathcal{O}(1)$  common in the literature, a runaway regime is quite likely. Note however that numerical studies have not been carried out in the ultra relativistic regime.

For deflagrations and hybrids, a significant fraction of the available energy goes into bulk fluid motions. On the other hand, for a non-steady state solution, a large fraction of the energy goes into accelerating the wall and little goes into bulk fluid motions, as seen in Fig. 12. Therefore, and perhaps counterintuitively, we find that, in a very strong first order phase transition, the contribution to the gravity wave spectrum from turbulent fluid flows is probably subdominant. While the overall size of the gravity wave signal is essentially controlled by the amount of vacuum energy released, i.e. by  $\alpha_N$ , its detailed spectrum will depend on how the energy is distributed among the different components (wall versus plasma). We have therefore provided the relation between the fluid velocity and the bubble wall velocity in Fig. 7. In addition, we estimated the thickness of the plasma shell near the bubble wall where the kinetic energy in the plasma is concentrated. In all numerical calculations of the GW background [4, 5, 10], it has been assumed for simplicity that all the energy was concentrated on the bubble surface and finite thickness effects were ignored (they were instead considered in the analytical approach of [9]). This is a reasonable approximation for detonations, although we show that even for supersonic wall velocities, the thickness of the plasma shell can reach  $\sim 20\%$  of the bubble size, see Fig. 9.

Finally, the nature of the electroweak phase transition is unknown and it will take some time before we can determine whether electroweak symmetry breaking is purely Standard Model-like or there are large deviations in the Higgs sector which could have led to a first-order phase transition. Although our analysis was implicitly motivated by the electroweak phase transition, it could be applicable to other first-order phase transitions in the early universe.

## Acknowledgment

We thank Dan Chung for mentioning the mismatch in the different definitions of efficiency factors to us. J.R.E. and J.M. No thank CERN TH-Division for partial financial support during different stages of this work. We acknowledge support from the European Commission the European Research Council Starting Grant Cosmo@LHC and the Marie Curie Research and Training Networks “ForcesUniverse” (MRTN-CT-2006-035863) and ‘UniverseNet’ (MRTN-CT-2006-035863); by the Spanish Consolider-Ingenio 2010 Programme CPAN (CSD2007-00042); the Comunidad Autónoma de Madrid under grant HEPHACOS P-ESP-00346 and the Spanish Ministry MICNN under contract FPA 2007-60252.



## A Numerical fits to the efficiency coefficients

In this section we provide fits to the numerical results of section 4. These fits facilitate the functions  $\kappa(\xi_w, \alpha_N)$  and  $\alpha_+(\xi_w, \alpha_N)$  without solving the flow equations and with a precision better than 15% in the region  $10^{-3} < \alpha_N < 10$ .

In order to fit the function  $\kappa(\xi_w, \alpha_N)$ , we split the parameter space into three regions and provide approximations for the four boundary cases and three families of functions that interpolate in-between: For small wall velocities one obtains ( $\xi_w \ll c_s$ )

$$\kappa_A \simeq \xi_w^{6/5} \frac{6.9\alpha_N}{1.36 - 0.037\sqrt{\alpha_N} + \alpha_N} . \quad (95)$$

For the transition from subsonic to supersonic deflagrations ( $\xi_w = c_s$ )

$$\kappa_B \simeq \frac{\alpha_N^{2/5}}{0.017 + (0.997 + \alpha_N)^{2/5}} . \quad (96)$$

For Jouguet detonations ( $\xi_w = \xi_J$ ), as stated in eq. (40)

$$\kappa_C \simeq \frac{\sqrt{\alpha_N}}{0.135 + \sqrt{0.98 + \alpha_N}} \quad \text{and} \quad \xi_J = \frac{\sqrt{\frac{2}{3}\alpha_N + \alpha_N^2} + \sqrt{1/3}}{1 + \alpha_N} . \quad (97)$$

And finally for very large wall velocity, ( $\xi_w \rightarrow 1$ ) as stated in eq. (42)

$$\kappa_D \simeq \frac{\alpha_N}{0.73 + 0.083\sqrt{\alpha_N} + \alpha_N} . \quad (98)$$

For subsonic deflagrations a good fit to the numerical results is provided by

$$\kappa(\xi_w \lesssim c_s) \simeq \frac{c_s^{11/5} \kappa_A \kappa_B}{(c_s^{11/5} - \xi_w^{11/5}) \kappa_B + \xi_w c_s^{6/5} \kappa_A} , \quad (99)$$

and for detonations by

$$\kappa(\xi_w \gtrsim \xi_J) \simeq \frac{(\xi_J - 1)^3 \xi_J^{5/2} \xi_w^{-5/2} \kappa_C \kappa_D}{[(\xi_J - 1)^3 - (\xi_w - 1)^3] \xi_J^{5/2} \kappa_C + (\xi_w - 1)^3 \kappa_D} . \quad (100)$$

The numerical result for the hybrid (supersonic deflagration) region is well described by a cubic polynomial. As boundary conditions, one best uses the two values of  $\kappa$  and the first derivative of  $\kappa$  at  $\xi_w = c_s$ . Notice that the derivative of  $\kappa$  in  $\xi_w$  is not continuous at the point  $\xi_J$ . The derivative at  $\xi_w = c_s$  is approximately given by

$$\delta\kappa \simeq -0.9 \log \frac{\sqrt{\alpha_N}}{1 + \sqrt{\alpha_N}} . \quad (101)$$

This differs from the derivative one would obtain from the fit in the region  $\xi_w < c_s$ , but mostly for values  $\alpha \gtrsim 1$ , where no solutions exist for  $\xi_w < c_s$ . The expression for supersonic deflagrations then reads

$$\kappa(c_s < \xi_w < \xi_J) \simeq \kappa_B + (\xi_w - c_s) \delta\kappa + \frac{(\xi_w - c_s)^3}{(\xi_J - c_s)^3} [\kappa_C - \kappa_B - (\xi_J - c_s) \delta\kappa] . \quad (102)$$

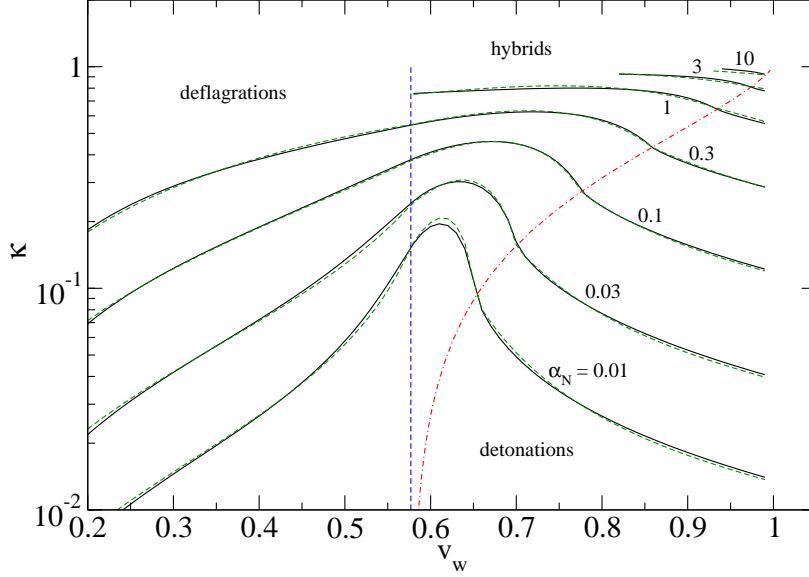


Figure 13: The efficiency coefficient  $\kappa$  as a function of the wall velocity  $\xi_w$  for fixed  $\alpha_N$  and the fit (dashed lines) described in the text.

The fits of  $\kappa$  compared to the numerical results are given in Fig. 13. The relative errors never exceed 15%.

Another useful function is the maximal  $\alpha_N$  that can be realized for fixed  $\xi_w$ . This function is approximately given by

$$\alpha_N^{max} \simeq \frac{1}{3}(1 - \xi_w)^{-13/10}. \quad (103)$$

Finally, the connection between  $\alpha_N$  and  $\alpha_+$  might be needed in phenomenological studies. Like in the case for  $\kappa$ , we provide approximations or analytic expressions in limiting cases and interpolate in between. For velocities larger than the Jouguet velocity  $\xi_J$ ,  $\alpha_+$  and  $\alpha_N$  coincide. For  $\alpha_N < 1/3$  all velocities can be realized and in this case the limit  $v_w \rightarrow 0$  also yields  $\alpha_+ \rightarrow \alpha_N$ . Otherwise there is a minimal  $\xi_w$  which is, according to eq. (103), given by

$$\alpha_+ = 1/3 \quad \text{for} \quad \xi_w = 1 - (3\alpha_N)^{-10/13} \quad \text{if} \quad \alpha_N > \frac{1}{3}. \quad (104)$$

For relatively small  $\alpha_N$  a wall velocity of the speed of sound can be realized leading to a fit

$$\begin{aligned} \alpha_+(c_s) &\simeq \alpha_N(0.329 - 0.0793 \log \alpha_N + 0.0116 \log^2 \alpha_N + 0.00159 \log^3 \alpha_N) \\ &\text{if} \quad \alpha_N < \frac{1}{3}(1 - c_s)^{-13/10} \simeq 1.02. \end{aligned} \quad (105)$$

Finally, the transition from supersonic deflagrations to detonations can be determined analytically leading to

$$\alpha_+(\xi_J) = \alpha_N \frac{3 - 3\xi_J^2}{9\xi_J^2 - 1} \quad \text{for all} \quad \alpha_N. \quad (106)$$

For  $\alpha_N > 1/3$ , the function  $\alpha_+(\alpha_N, \xi_w)$  is well approximated by a polynomial in  $\xi_w$  that contains the two/three data points just given for the case  $\alpha_N \gtrless 1.02$ . For  $\alpha_N < 1/3$ , the

function  $\alpha_+(\alpha_N, \xi_w)$  is approximately linear in the region  $\xi_w \in [c_s, \xi_J]$  and goes slowly to  $\alpha_N$  for  $\xi_w \rightarrow 0$ . For velocities below  $c_s$ , a reasonable approximation is of the form

$$\alpha_+ = \frac{\alpha_N + c_1 \xi_w^2}{1 + c_2 \xi_w^2}, \quad (107)$$

and matching of this function and its derivative to the linear regime yields

$$\alpha_+ = \frac{(c_s^2 - \xi_w^2)[\alpha_+(\xi_J) - \alpha_+(c_s)]\alpha_N - 2\xi_w^2(1 - \xi_J/c_s)[\alpha_+(c_s) - \alpha_N]\alpha_+(c_s)}{(c_s^2 - \xi_w^2)[\alpha_+(\xi_J) - \alpha_+(c_s)] - 2\xi_w^2(1 - \xi_J/c_s)[\alpha_+(c_s) - \alpha_N]}. \quad (108)$$

The comparison between fit and numerical results is given in Fig. 14. The relative error never exceeds 5% and is worst for  $\alpha_N \sim 0.3$ .

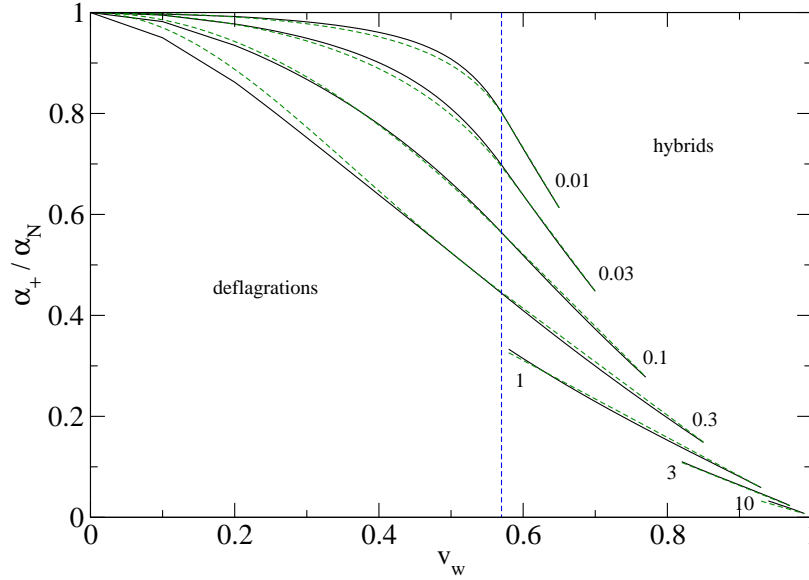


Figure 14: The ratio  $\alpha_+/\alpha_N$  as a function of the wall velocity  $\xi_w$  for fixed  $\alpha_N$  and the fit (dashed lines) described in the text.

## References

- [1] The mechanism was first worked out in: A. G. Cohen, D. B. Kaplan and A. E. Nelson, Phys. Lett. B **245** (1990) 561; Nucl. Phys. B **349** (1991) 727; Nucl. Phys. B **373** (1992) 453; Phys. Lett. B **336** (1994) 41 [hep-ph/9406345]. For a review see e.g J. M. Cline, [hep-ph/0609145].
- [2] C. J. Hogan, Phys. Rev. Lett. **51** (1983) 1488; J. M. Quashnock, A. Loeb and D. N. Spergel, Astrophys. J. Lett. **344**: L49 (1989); T. Vachaspati, Phys. Lett. B **265**, 258 (1991); B. I. Cheng and A. V. Olinto, Phys. Rev. D **50**, 2421 (1994); G. Baym, D. Bodeker and L. D. McLerran, Phys. Rev. D **53** (1996) 662 [hep-ph/9507429].

- [3] E. Witten, Phys. Rev. D **30**, 272 (1984); C. Hogan, MNRAS **218**, 629, 1986.
- [4] A. Kosowsky, M. S. Turner and R. Watkins, Phys. Rev. D **45** (1992) 4514; Phys. Rev. Lett. **69**, 2026 (1992); A. Kosowsky and M. S. Turner, Phys. Rev. D **47** (1993) 4372 [astro-ph/9211004].
- [5] M. Kamionkowski, A. Kosowsky and M. S. Turner, Phys. Rev. D **49** (1994) 2837 [astro-ph/9310044].
- [6] L. D. Landau and E. M. Lifshitz, “Fluid Mechanics,” Pergamon Press, New York, 1989.
- [7] P. J. Steinhardt, Phys. Rev. D **25** (1982) 2074.
- [8] R. Apreda, M. Maggiore, A. Nicolis and A. Riotto, Nucl. Phys. B **631** (2002) 342 [gr-qc/0107033]; A. Nicolis, Class. Quant. Grav. **21** (2004) L27 [gr-qc/0303084]; C. Grojean and G. Servant, Phys. Rev. D **75** (2007) 043507 [hep-ph/0607107]; L. Randall and G. Servant, JHEP **0705** (2007) 054 [arXiv:hep-ph/0607158]; S. J. Huber and T. Konstandin, JCAP **0805** (2008) 017 [hep-ph/0709.2091]; T. Kahniashvili, A. Kosowsky, G. Gogoberidze and Y. Maravin, Phys. Rev. D **78** (2008) 043003 [astro-ph/0806.0293].
- [9] C. Caprini, R. Durrer and G. Servant, Phys. Rev. D **77** (2008) 124015 [astro-ph/0711.2593];
- [10] S. J. Huber and T. Konstandin, JCAP **0809** (2008) 022 [hep-ph/0806.1828];
- [11] C. Caprini, R. Durrer, T. Konstandin and G. Servant, [astro-ph/0901.1661].
- [12] A. Kosowsky, A. Mack and T. Kahniashvili, Phys. Rev. D **66** (2002) 024030 [astro-ph/0111483]; A. D. Dolgov, D. Grasso and A. Nicolis, Phys. Rev. D **66** (2002) 103505 [astro-ph/0206461]; G. Gogoberidze, T. Kahniashvili and A. Kosowsky, Phys. Rev. D **76** (2007) 083002 [astro-ph/0705.1733].
- [13] C. Caprini and R. Durrer, Phys. Rev. D **74** (2006) 063521 [astro-ph/0603476]; C. Caprini, R. Durrer and G. Servant, JCAP **0912** (2009) 024 [astro-ph.CO/0909.0622].
- [14] M. Laine, Phys. Rev. D **49** (1994) 3847 [hep-ph/9309242].
- [15] G. D. Moore and T. Prokopec, Phys. Rev. D **52** (1995) 7182 [hep-ph/9506475].
- [16] J. Ignatius, K. Kajantie, H. Kurki-Suonio and M. Laine, Phys. Rev. D **49** (1994) 3854 [astro-ph/9309059].
- [17] H. Kurki-Suonio, Nucl. Phys. B **255** (1985) 231.
- [18] M. Gyulassy, K. Kajantie, H. Kurki-Suonio and L. D. McLerran, Nucl. Phys. B **237**, 477 (1984); K. Kajantie and H. Kurki-Suonio, Phys. Rev. D **34**, 1719 (1986); K. Enqvist, J. Ignatius, K. Kajantie and K. Rummukainen, Phys. Rev. D **45** (1992) 3415; M. Dine, R. G. Leigh, P. Y. Huet, A. D. Linde and D. A. Linde, Phys. Rev. D **46** (1992) 550 [hep-ph/9203203]; B. H. Liu, L. D. McLerran and N. Turok, Phys. Rev. D **46** (1992) 2668; P. Y. Huet, K. Kajantie, R. G. Leigh, B. H. Liu and L. D. McLerran, Phys. Rev.

- D **48** (1993) 2477 [hep-ph/9212224]; J. C. Miller and L. Rezzolla, Phys. Rev. D **51** (1995) 4017 [astro-ph/9411091].
- [19] H. Kurki-Suonio and M. Laine, Phys. Rev. D **51**, 5431 (1995) [hep-ph/9501216].
  - [20] P. John and M. G. Schmidt, Nucl. Phys. B **598** (2001) 291 [Erratum-ibid. B **648** (2003) 449] [hep-ph/0002050].
  - [21] J. M. Cline, M. Joyce and K. Kainulainen, JHEP **0007** (2000) 018 [hep-ph/0006119].
  - [22] M. S. Carena, J. M. Moreno, M. Quiros, M. Seco and C. E. M. Wagner, Nucl. Phys. B **599** (2001) 158 [hep-ph/0011055].
  - [23] M. S. Carena, M. Quiros, M. Seco and C. E. M. Wagner, Nucl. Phys. B **650** (2003) 24 [hep-ph/0208043].
  - [24] T. Konstandin, T. Prokopec, M. G. Schmidt and M. Seco, Nucl. Phys. B **738** (2006) 1 [hep-ph/0505103].
  - [25] V. Cirigliano, S. Profumo and M. J. Ramsey-Musolf, JHEP **0607**, 002 (2006) [hep-ph/0603246].
  - [26] A. Megevand and A. D. Sanchez, [hep-ph/0904.1753]; Nucl. Phys. B **825** (2010) 151 [hep-ph/0908.3663].
  - [27] D. Bodeker and G. D. Moore, JCAP **0905** (2009) 009 [hep-ph/0903.4099].
  - [28] G. D. Moore, JHEP **0003** (2000) 006 [arXiv:hep-ph/0001274].
  - [29] B. H. Liu, L. D. McLerran and N. Turok, Phys. Rev. D **46** (1992) 2668.
  - [30] M. Dine, R. G. Leigh, P. Y. Huet, A. D. Linde and D. A. Linde, Phys. Rev. D **46** (1992) 550 [arXiv:hep-ph/9203203].
  - [31] P. B. Arnold, Phys. Rev. D **48** (1993) 1539 [arXiv:hep-ph/9302258].
  - [32] T. Prokopec, M. G. Schmidt and S. Weinstock, Annals Phys. **314** (2004) 208 [hep-ph/0312110]; Annals Phys. **314** (2004) 267 [hep-ph/0406140].